

**MATHEMATICAL MODELING OF THE OVERALL FLOTATION DEINKING PROCESS:  
PROBABILITY OF COLLISION IMPROVEMENTS**

**Project F00903**

**Report 4**

**to the**

**MEMBER COMPANIES OF THE INSTITUTE OF PAPER SCIENCE AND TECHNOLOGY**

**January 15, 1998**

INSTITUTE OF PAPER SCIENCE AND TECHNOLOGY

Atlanta, Georgia

MATHEMATICAL MODELING OF THE OVERALL FLOTATION DEINKING PROCESS:  
PROBABILITY OF COLLISION IMPROVEMENTS

Project F00903

Report 4

A Progress Report

to the

MEMBER COMPANIES OF THE INSTITUTE OF PAPER SCIENCE AND TECHNOLOGY

By

T.J. Heindel and F. Bloom

January 15, 1998



## TABLE OF CONTENTS

1 Executive Summary .....	1
2 Introduction .....	2
3 The Probability of Collision ( $P_c$ ) .....	3
3.1 Theoretical Development .....	3
3.2 $P_c$ Predictions .....	18
3.2.1 Fixed $ G $ Predictions .....	19
3.2.2 Fixed $R_{e_B}$ Predictions .....	21
3.2.3 Fixed $R_p/R_B$ Predictions .....	23
3.2.4 Comparisons with Published Data .....	23
4 Conclusions .....	28
5 References .....	30
6 Nomenclature .....	32
7 Appendices .....	36
7.1 Appendix A: Exact and Approximate Collision Probabilities for Potential Flow .....	36
7.2 Appendix B: The Anfruns and Kitchener Results for $P_c$ .....	38
8 Figures .....	40



# 1 Executive Summary

This report revisits the flotation microprocess of collision and develops an exact expression for the probability of collision ( $P_c$ ) based on the intermediate flow of Yoon and Luttrell. This expression only assumes that the bubble and particle are spherical and that  $R_p < R_B$ . The expression developed here removes the additional assumptions that are typically invoked in the literature (i.e.,  $R_p + R_B \approx R_B$  and  $(R_p/R_B)^3 \ll (R_p/R_B)^2$ ). In addition to removing these restrictions from the expression for  $P_c$ , we also include the possibility that the particle settling velocity may also influence the collision probability.

The expression for  $P_c$  developed in this report is a function of three dimensionless groups: (i) the magnitude of the dimensionless particle settling velocity,  $|G|$ ; (ii) the bubble Reynolds number,  $Re_B$ ; and (iii) the ratio of particle-to-bubble size,  $R_p/R_B$ . This expression was then used to predict  $P_c$  for selected parametric ranges of  $0 \leq |G| \leq 5$ ,  $0 \leq Re_B \leq 500$ , and  $0.001 \leq R_p/R_B \leq 1$ .

In general,  $P_c$  is independent of  $Re_B$  when  $R_p/R_B \lesssim 0.05$  for all values of  $|G|$ . Conversely,  $P_c$  is not significantly influenced by  $|G|$  as  $R_p/R_B \rightarrow 1$  for all values of  $Re_B$ . The additional assumptions typically employed in the literature (i.e.,  $R_p + R_B \approx R_B$  and  $(R_p/R_B)^3 \ll (R_p/R_B)^2$ ) are valid only when  $R_p/R_B \lesssim 0.05 - 0.1$ , depending on the values of  $|G|$  and  $Re_B$ .

Finally, the new prediction for  $P_c$  presented here was compared to available experimental  $P_c$  data from the mineral processing industry. This new expression does a very good job at predicting measured  $P_c$  values. The inclusion of the particle settling velocity is very important, particularly when the particles have a density much higher than that of water. Additionally, the form of  $P_c$  derived from basic principles in this report is much simpler than that recently proposed by another researcher and it is just as accurate at predicting experimental results.

## 2 Introduction

Flotation deinking is a macroseparation process comprised of four microprocesses that must take place sequentially: (i) capture or collision of the ink particle by an air bubble; (ii) adhesion of the ink particle to the air bubble as it slides over the bubble surface; (iii) extension of a three-phase contact at the bubble/particle/liquid interface; and (iv) stabilization/destabilization of the bubble/particle aggregate. Report 1 of this project (1) summarized the microprocesses in great detail and presented available probability equations for each microprocess. These microprocess probabilities were used to develop a first-generation model of the overall flotation deinking process, which was also elaborated upon in Report 1 (1). This model was used in Report 2 of this project (2) to predict flotation efficiency and other flotation performance parameters for selected parametric ranges.

This current report revisits the first microprocess necessary for successful particle removal by flotation - the probability of collision ( $P_c$ ), and develops a new expression for  $P_c$  that is less restrictive and more accurate than those available in the literature. Predictions are then presented as a function of the magnitude of the dimensionless particle settling velocity,  $|G|$ , the bubble Reynolds number,  $Re_B$ , and the ratio of the particle-to-bubble size,  $R_p/R_B$ . Additional calculations have been performed to compare our predictive equation for  $P_c$  with available experimental data from the mineral processing industry.

The second microprocess necessary for successful particle removal by flotation, the probability of adhesion (or attachment) by sliding ( $P_{asl}$ ) will be reevaluated in a subsequent report, where a new expression for  $P_{asl}$  will be developed.

## 3 The Probability of Collision

### 3.1 Theoretical Development

In this section we will revisit expressions for  $P_c$ , the microprocess probability of capture of a particle by a bubble, which were originally presented in Report 1 (1), and develop improved expressions for this microprocess probability. In the analysis to follow, all particles and all bubbles in any given volume of the flotation cell are assumed to be perfectly spherical.

As indicated in Fig. 1, only those particles which approach a rising bubble within a streaming tube of limiting capture radius  $R_c$  can collide with or be intercepted by a bubble. Once an expression has been determined for  $R_c$ , the probability  $P_c$  is then computed to be the ratio of the number of particles with  $R_p < R_B$  which encounter a bubble per unit time to the number of particles which approach a bubble in a stream tube with cross section equal to  $\pi(R_p + R_B)^2$ ; this ratio is easily determined to be given by

$$P_c = \left( R_c / (R_p + R_B) \right)^2 \quad [3.1]$$

Many authors simply take  $P_c = \left( R_c / R_B \right)^2$ , e.g. Yoon and Luttrell (4); however, as these authors note, “the denominator should actually be  $R_B + R_p$  but (the) equation holds when  $R_B \gg R_p$ ”. Because one of our goals is the derivation of exact expressions for  $P_c$ , we choose not to make any approximations which are based upon assumptions concerning the relative magnitudes of  $R_p$  and  $R_B$  until the final stages of the analysis.

The determination of an expression for  $R_c$  in [3.1] is a nontrivial exercise which has occupied the attention of many researchers in colloidal hydrodynamics during the past six decades since the original work of Sutherland (3) (which dealt with potential flow around the bubble in the absence of both inertial forces and gravitational effects); principal contri-

butions in this area include the work of Yoon and Luttrell (4, 5), Ahmed and Jameson (6), Schulze (7, 8), Flint and Howarth (9), Nguyen-Van and Kmet (10), Nguyen-Van (11), Weber (12), Weber and Paddock (13), Reay and Ratcliff (14), Dobby and Finch (15), Anfruns and Kitchener (16, 17), Spielman (18), and Michael and Norey (19). During the course of the analysis to follow here, we will have occasion to refer to specific results in several of the papers referenced above and, in particular, will indicate the manner in which many of those results are either special cases of or approximations to the more exact relations that are derived below.

The specific derivation of expressions for the capture radius  $R_c$  is dependent upon the basic assumptions one makes about the relationship between  $R_p$  and  $R_B$ , the nature of the flow field in which the particle moves, and the role (or lack thereof) of inertial and gravitational forces in the process. At this stage of the overall flotation process, i.e., the approach of a particle to a bubble, only the long-range hydrodynamic interaction is taken into account as opposed to those short-range hydrodynamic interactions which must be considered once the particle has intercepted the bubble and begins the sliding process over the thin film which surrounds the bubble surface. A rather comprehensive discussion of the overall flotation deinking process may be found in the recent papers (20-22) of the authors as well as in the reports (1, 2).

Among the key parameters which arise in any discussion of the flow field in the neighborhood of a rising bubble are the bubble Reynolds number

$$Re_B = \frac{v_B d_B \rho_\ell}{\mu_\ell} \quad [3.2]$$

and the Stokes number

$$St = \frac{\rho_p d_p^2 v_B}{9\mu_\ell d_B} = \frac{Re_B \rho_p d_p^2}{9\rho_\ell d_B^2} \quad [3.3]$$

which is the ratio of the inertial force of the particle to the viscous drag force of the bubble. Much of the earlier literature on flotation processes was concerned with mineral flotation for which  $0.1 < St < 1$  is a reasonable assumption; however, some of the later work in that area, as well as almost all the work on flotation deinking, has been concerned with the situation in which  $St \ll 0.1$  so that inertial forces, in essence, no longer influence particle motion. Under these circumstances, it is still possible for particle paths to deviate slightly from the streamlines of the flow if one accounts for particle settling velocity.

In the present work three types of flow will be discussed: potential flow, Stokes flow, and the intermediate flow of Yoon and Luttrell (4, 5); our main interest is in the latter class of flows as previously discussed in, e.g., (20); the class of intermediate flows introduced in (4) has also been incorporated into the work, e.g., of Schulze (7) and Nguyen-Van (11) and discussed in the recent survey paper of Matis and Zouboulis (23). For all three of the flows listed above we shall assume that the flow streamlines are symmetrical, fore and aft, with respect to the bubble surface; such an assumption was explicitly employed by Yoon and Luttrell (4) and implies that a grazing trajectory may be defined as the one which, at the equator, passes within a distance of particle radius  $R_p$  from the bubble surface (Fig. 2.). Clearly, such a trajectory, when traced back an infinite distance from the bubble surface, passes precisely within a distance  $R_c$  of the stagnation line of the flow which passes through the bubble center. If one does not assume that the grazing trajectory occurs at  $\theta = \frac{\pi}{2}$  in Fig. 2., then a collision angle  $\theta_c$  must be introduced,  $\theta_c$  being the angle on the bubble surface, measured from the front stagnation point, over which particle interception by the surface is possible. The recent work of Nguyen-Van (11) indicates that  $\theta_c = \pi/2$  for the intermediate flow of Yoon and Luttrell (4), as well as for potential flow and creeping Stokes flow, is a reasonable assumption. Cases for which  $\theta_c \neq \pi/2$  have been discussed in, e.g., (10-15).

In order to determine the trajectory of a particle approaching a rising bubble, we begin by considering, in Cartesian coordinates, the forces which act on a typical particle. Let  $\mathbf{v}_p$  represent the particle velocity,  $v_{px}$  and  $v_{py}$ , the  $x$  and  $y$  components, respectively, of the velocity field of the particle, and  $m$  the inertial mass of the particle; then, in general,

$$\begin{cases} m \frac{dv_{px}}{dt} = -F_{dx} \\ m \frac{dv_{py}}{dt} = (F_g - F_b) - F_{dy} \end{cases} \quad [3.4]$$

In [3.4],  $F_{dx}$  and  $F_{dy}$  represent the  $x$  and  $y$  components of the drag force, respectively, (Fig. 3.) and  $F_g - F_b$  is the differences between the gravitational and buoyancy forces which act on the particle as it approaches a bubble. The system [3.4] may be written in the form

$$\begin{cases} \frac{4}{3} \pi \rho_p R_p^3 \frac{dv_{px}}{dt} = -f(v_{px} - u_x) \\ \frac{4}{3} \pi \rho_p R_p^3 \frac{dv_{py}}{dt} = \frac{4}{3} \pi R_p \Delta \rho g - f(v_{py} - u_y) \end{cases} \quad [3.5]$$

where  $f$  is the friction factor and  $\Delta \rho = \rho_p - \rho_\ell$ . For Stokesian particles it is well know that  $f = 6\pi\mu_\ell R_p$  in which case the drag force is given by  $\mathbf{F}_d = 6\pi\mu_\ell R_p \mathbf{v}_p$ . For non-Stokesian particles we have, in general,  $\mathbf{F}_d = f \mathbf{v}_p$  while the coefficient of drag,  $C_D$ , is defined to be

$$C_D \equiv \frac{|\mathbf{F}_d|}{\frac{1}{2} \rho_\ell |\mathbf{v}_p|^2 \pi R_p^2} \quad [3.6]$$

or, in view of the definition of  $\mathbf{F}_d$  in terms of  $f$ ,

$$C_D = \frac{f}{\frac{1}{2} \rho_\ell |\mathbf{v}_p| \pi R_p^2} \quad [3.7]$$

In the Stokesian case, with  $f = 6\pi\mu_\ell R_p$  and  $C_D = C_D^{st}$ , [3.7] yields

$$C_D^{st} = 12\nu_\ell / R_p |\mathbf{v}_p| \quad [3.8]$$

If we define, in the usual manner, the Reynolds number for the particle to be

$$Re_p = \frac{2R_p|\mathbf{v}_p|}{\nu_\ell} \quad [3.9]$$

then [3.8], [3.9] yield the widely known result (e.g., Cheremisinoff (24)) that  $C_D^{st} = 24/Re_p$ .

In the general case, however, it is easily seen that [3.7], [3.9] combine so as to yield

$$C_D = \frac{4f}{(\pi\mu_\ell R_p)Re_p} \quad [3.10]$$

It is generally accepted (e.g. (24)) that  $C_D = C_D^{st} = 24/Re_p$  holds for  $Re_p < 2$ . For the situation that is considered below, in which inertial forces acting on the particle are ignored (so that, in effect, the Stokes number  $St = 0$ ), the particle velocity corresponds to the particle settling velocity ( $\mathbf{v}_p = \mathbf{v}_{ps}$ ). In this case it can be demonstrated (i.e., (24)) that

$$C_D Re_p^2 = \frac{4}{3} Ar \quad [3.11]$$

where the Archimedes number  $Ar$  is the dimensionless parameter defined by

$$Ar = \frac{\Delta\rho d_p^3 g}{\rho_\ell \nu_\ell^2} \quad [3.12]$$

For the Stokes' law range ( $Re_p < 2$ ), the use of  $C_D = C_D^{st} = \frac{24}{Re_p}$  in [3.11] leads to  $Re_p = \frac{Ar}{18}$ , i.e., the Stokesian regime with respect to particle settling velocity corresponds to  $Ar < 36$ .

In the intermediate or transitional range in which  $2 < Re_p < 500$  empirical results must be used; from the results reported in (24), we infer that

$$C_D = \frac{18.5}{Re_p^{0.6}}, \quad 2 < Re_p < 500 \quad [3.13]$$

the use of which in [3.11] yields

$$Re_p = 0.152 Ar^{0.715}, \quad 2 < Re_p < 500 \quad [3.14]$$

By combining [3.10] with [3.13], solving for  $f$ , and then using [3.14] to eliminate  $Re_p$ , one may express, for the case  $St = 0$ , the friction factor  $f$  in terms of the Archimedes number  $Ar$ , the fluid viscosity  $\mu_\ell$ , and the particle radius  $R_p$ . In fact, by combining [3.10] with [3.11] we find that, in general

$$f = \frac{\pi\mu_\ell R_p}{3} \frac{Ar}{Re_p} \quad [3.15]$$

From [3.15], with  $Re_p = \frac{Ar}{18}$  for Stokesian particles, we recover the usual friction factor  $f = 6\pi\mu_\ell R_p$  associated with the Stokes flow regime, while for  $2 < Re_p < 500$  the required result for  $f$  is obtained by combining [3.15] with the empirical relation [3.14].

For the analysis which follows it is convenient to introduce the dimensionless factor

$$\begin{aligned} \lambda &\equiv 6\pi\mu_\ell R_p / f \\ &= 18Re_p / Ar \end{aligned} \quad [3.16]$$

by virtue of [3.15]. Clearly  $\lambda = 1$  for Stokesian particles ( $Re_p < 2$ ) while in the transitional domain ( $2 < Re_p < 500$ )  $\lambda$  may be computed by combining [3.16] with the empirical relation [3.14].

We now return to the system [3.5] and nondimensionalize the equations by introducing the variables

$$\mathbf{v}_p^* = \frac{\mathbf{v}_p}{v_B}, \quad \mathbf{u}^* = \frac{\mathbf{u}}{v_B}, \quad t^* = \frac{tv_B}{R_B} \quad [3.17]$$

A straightforward calculation yields the system

$$\begin{cases} St \frac{dv_{px}^*}{dt^*} = -\frac{f}{6\pi\mu_\ell R_p} (v_{px}^* - u_x^*) \\ St \frac{dv_{py}^*}{dt^*} = \frac{2R_p^2 \Delta\rho g}{9\mu_\ell v_B} - \frac{f}{6\pi\mu_\ell R_p} (v_{py}^* - u_y^*) \end{cases}$$

or upon introducing the dimensionless friction factor  $\lambda$  as given by [3.16],

$$\begin{cases} \lambda St \frac{dv_{px}^*}{dt^*} = -(v_{px}^* - u_x^*) \\ \lambda St \frac{dv_{py}^*}{dt} = \frac{2R_p^2 \Delta\rho g}{9\mu_\ell v_B} \lambda - (v_{py}^* - u_y^*) \end{cases} \quad [3.18]$$

We now set

$$\tilde{v}_{ps} = -\frac{2R_p^2 \Delta\rho g}{9\mu_\ell} \quad [3.19a]$$

and

$$G = \lambda \frac{\tilde{v}_{ps}}{v_B} \equiv \frac{v_{ps}}{v_B} \quad [3.19b]$$

According to our sign convention  $v_B > 0$  so that  $v_{ps} < 0$ ; thus, we also have  $G < 0$ . In [3.19],  $\tilde{v}_{ps}$  represents the (terminal) particle settling velocity for Stokesian particles,  $v_{ps} = \lambda \tilde{v}_{ps}$  is the true particle settling velocity, and  $G$  is the dimensionless particle settling velocity. For Stokesian particles, therefore,  $G = \tilde{v}_{ps}/v_B$ .

Using the definitions [3.19], in [3.18], assuming that  $St \simeq 0$ , so that inertial effects are discounted, and noting that  $-v_{ps} = |v_{ps}|$ ,  $-G = |G|$ , we easily find that

$$\begin{cases} v_{px}^* = u_x^* \\ v_{py}^* = |G| + u_y^* \end{cases} \quad [3.20]$$

The system [3.20] has previously appeared in Flint and Howarth (9) and Schulze (8); however, in these references it has been assumed that  $G \equiv \tilde{v}_{ps}/v_B$ , which is only valid for Stokes flow.

We begin the analysis by recalling that in [3.1]  $R_c$  represents the largest distance from the stagnation line through the center of the rising bubble, within which a particle path trajectory can pass so that the particle surface will graze the bubble surface at  $\theta = \pi/2$ , i.e.,

the maximal distance so that  $r = R_B + R_p$  along the particle path trajectory when  $\theta = \pi/2$ . By virtue of [3.20], particle path trajectories are coincident with fluid flow streamlines when  $G = 0$ . Also, from Fig. 2, it is clear that there exists a smallest  $r$ , say,  $r = r_c$  with the property that, along a particle path trajectory, an approaching particle will be at the distance  $R_c$  from the stagnation line through the center of a rising bubble for all  $r \geq r_c$ . We now define  $\theta_0$  by

$$\sin \theta_0 = R_c/r_c \quad [3.21]$$

and note that

$$\sin \theta = \frac{R_c}{r}, \quad \text{for all } r \geq r_c \quad [3.22]$$

Our first task is the derivation of an exact expression for  $P_c$  for the case of the intermediate flow delineated in Yoon and Luttrell (4). The stream function for ‘intermediate flow’ (as given in (4)), has the form

$$\begin{aligned} \psi^{int} = v_B R_B^2 \sin^2 \theta & \left[ \frac{1}{2} r^{*2} - \frac{3}{4} r^* + \frac{1}{4r^*} \right. \\ & \left. + Re_B^* \left( \frac{1}{r^{*2}} - \frac{1}{r^*} + r^* - 1 \right) \right] \end{aligned} \quad [3.23]$$

where

$$Re_B^* = \frac{1}{15} Re_B^{0.72}, \quad r^* = r/R_B \quad [3.24]$$

The expression [3.23] for  $\psi^{int}$  is obtained in (4) by using the (empirically deduced) value

$$\hat{\alpha} = 1 - \frac{4}{3} Re_B^* \left( 1 - \frac{1}{r^*} \right) \quad [3.25]$$

in the expression

$$\psi^{int} = v_B R_B^2 \sin^2 \theta \left[ \frac{1}{2} r^{*2} - \frac{3}{4} \hat{\alpha} r^* - \frac{1}{2r^*} + \frac{3\hat{\alpha}}{4r^*} \right] \quad [3.26]$$

For  $\hat{\alpha} = 0$ , [3.26] yields the stream function for potential flow,

$$\psi^{pot} = v_B R_B^2 \sin^2 \theta \left[ \frac{1}{2} r^{*2} - \frac{1}{2r^*} \right] \quad [3.27]$$

while for  $\hat{\alpha} = 1$ , [3.26] yields

$$\psi^{st} = v_B R_B^2 \sin^2 \theta \left[ \frac{1}{2} r^{*2} - \frac{3}{4} r^* + \frac{1}{4r^*} \right] \quad [3.28]$$

which is the stream function for Stokes flow. In fact, it is easily seen that [3.26] is obtained by direct interpolation between  $\psi^{pot}$  and  $\psi^{st}$ , i.e.

$$\begin{aligned} \hat{\alpha} \psi^{st} + (1 - \hat{\alpha}) \psi^{pot} = \\ \hat{\alpha} v_B R_B^2 \sin^2 \theta \left[ \frac{1}{2} r^{*2} - \frac{3}{4} r^* + \frac{1}{4r^*} \right] \\ + (1 - \hat{\alpha}) v_B R_B^2 \sin^2 \theta \left[ \frac{1}{2} r^{*2} - \frac{1}{2r^*} \right] \equiv \psi^{int} \end{aligned} \quad [3.29]$$

if one algebraically combines like terms on the right-hand side of [3.29]. Setting  $r^* = r/R_B$  in [3.23] we have

$$\begin{aligned} \psi^{int} = v_B R_B^2 \sin^2 \theta \left[ \left( \frac{1}{2} \frac{r^2}{R_B^2} - \frac{3}{4} \frac{r}{R_B} + \frac{1}{4} \frac{R_B}{r} \right) \right. \\ \left. + Re_B^* \left( \frac{R_B^2}{r^2} - \frac{R_B}{r} + \frac{r}{R_B} - 1 \right) \right] \end{aligned} \quad [3.30]$$

Returning to [3.20] we rewrite this system of equations in ‘polar coordinates’ (actually, spherical coordinates projected onto the  $x, y$  plane) as

$$\begin{cases} v_{p\theta}^* = |G| \sin \theta + u_\theta^* \\ v_{pr}^* = -|G| \cos \theta + u_r^* \end{cases} \quad [3.31]$$

where

$$u_\theta^* = u_\theta / v_B, \quad u_r^* = u_r / v_B \quad [3.32]$$

The system [3.31] is identical to the similar (dimensionless) system in Flint and Howarth (9) except for the interpretation of  $G$  that has already been noted. The dimensional form of [3.31] is

$$\begin{cases} v_{p\theta} = u_\theta + v_B |G| \sin \theta \\ v_{pr} = u_r - v_B |G| \cos \theta \end{cases} \quad [3.33]$$

so that the radial and tangential components of the particle velocity field  $\mathbf{v}$  are computable once the radial and tangential components of the fluid velocity field have been specified; in [3.33],  $v_B G = v_{ps} \equiv \lambda \tilde{v}_{ps}$ , the (dimensional) particle settling velocity.

If  $\Psi^*$  is the dimensionless particle trajectory stream function (see, e.g., Batchelor (25), §2.2) then

$$\begin{cases} v_{p\theta}^* = \frac{1}{r^* \sin \theta} \frac{\partial \Psi^*}{\partial r^*} \\ v_{pr}^* = -\frac{1}{r^{*2} \sin \theta} \frac{\partial \Psi^*}{\partial \theta} \end{cases} \quad [3.34]$$

or, in dimensional form (with  $v_{p\theta}^* \rightarrow v_{p\theta}/v_B$ ,  $r^* \rightarrow r/R_B$ ,  $\partial/\partial r^* \rightarrow (1/R_B) \partial/\partial r$ )

$$\begin{cases} v_{p\theta} = v_B R_B^2 \frac{1}{r \sin \theta} \frac{\partial \Psi^*}{\partial r} = \frac{1}{r \sin \theta} \frac{\partial \Psi}{\partial r} \\ v_{pr} = -v_B R_B^2 \frac{1}{r^2 \sin \theta} \frac{\partial \Psi^*}{\partial \theta} = -\frac{1}{r^2 \sin \theta} \frac{\partial \Psi}{\partial \theta} \end{cases} \quad [3.35]$$

where the dimensional form of the particle trajectory stream function is given by

$$\Psi = v_B R_B^2 \Psi^* \quad [3.36]$$

If  $\mathbf{u}$  is the fluid velocity field which corresponds to the intermediate flow of Yoon and Luttrell (4), then by virtue of [3.33], [3.35] and [3.36].

$$\begin{cases} v_B R_B^2 \frac{1}{r \sin \theta} \frac{\partial \Psi^{*int}}{\partial r} = u_\theta^{int} + v_B |G| \sin \theta \\ -v_B R_B^2 \frac{1}{r^2 \sin \theta} \frac{\partial \Psi^{*int}}{\partial \theta} = u_r^{int} - v_B |G| \cos \theta \end{cases} \quad [3.37]$$

However,

$$\begin{cases} u_\theta^{int} = v_B R_B^2 \frac{1}{r \sin \theta} \frac{\partial \psi^{*int}}{\partial r} \\ u_r^{int} = -v_B R_B^2 \frac{1}{r^2 \sin \theta} \frac{\partial \psi^{*int}}{\partial \theta} \end{cases} \quad [3.38]$$

where, by virtue of [3.23],

$$\begin{aligned} \psi^{*int} = \sin^2 \theta \left[ \frac{1}{2} r^{*2} - \frac{3}{4} r^* + \frac{1}{4r^*} \right. \\ \left. + Re_B^* \left( \frac{1}{r^{*2}} - \frac{1}{r^*} + r^* - 1 \right) \right] \end{aligned} \quad [3.39]$$

By combining [3.37] and [3.38] we easily obtain the system

$$\begin{cases} \frac{\partial \Psi^{*int}}{\partial r} = \frac{\partial \psi^{*int}}{\partial r} + \frac{|G|}{R_B^2} r \sin \theta \\ \frac{\partial \Psi^{*int}}{\partial \theta} = \frac{\partial \psi^{*int}}{\partial \theta} + \frac{1}{2} \frac{|G|}{R_B^2} r^2 \sin 2\theta \end{cases} \quad [3.40]$$

We now (partially) integrate the first equation in [3.40] with respect to  $r$ , and the second with respect to  $\theta$ , so as to obtain

$$\begin{cases} \Psi^{*int} = \psi^{*int} + \frac{1}{2} \frac{|G|}{R_B^2} r^2 \sin^2 \theta + f(\theta) \\ \Psi^{*int} = \psi^{*int} - \frac{1}{4} \frac{|G|}{R_B^2} r^2 \cos 2\theta + h(r) \end{cases} \quad [3.41]$$

where,  $f$  and  $h$  are (at this point) arbitrary functions of their respective arguments. Substituting  $\cos 2\theta = 1 - 2\sin^2 \theta$  in the second equation in [3.41], and comparing the expressions for  $\Psi^{*int}$ , we are led to the conclusion that  $f(\theta) = 0$ ,  $h(r) = \frac{1}{4} \frac{|G|}{R_B^2} r^2$  and

$$\Psi^{*int} = \psi^{*int} + \frac{1}{2} \frac{|G|}{R_B^2} r^2 \sin^2 \theta \quad [3.42]$$

Combining [3.42] with [3.39], we obtain for the particle trajectory stream function associated with the intermediate flow of Yoon and Luttrell (4)

$$\begin{aligned} \Psi^{*int} = \sin^2 \theta \left\{ \left[ \frac{1}{2} r^{*2} (1 + |G|) - \frac{3}{4} r^* + \frac{1}{4r^*} \right] \right. \\ \left. + Re_B^* \left[ \frac{1}{r^{*2}} - \frac{1}{r^*} + r^* - 1 \right] \right\} \end{aligned} \quad [3.43]$$

or, in dimensional form,

$$\begin{aligned} \Psi^{int} = v_B R_B^2 \sin^2 \theta \left\{ \left[ \frac{1}{2} (1 + |G|) \frac{r^2}{R_B^2} - \frac{3}{4} \frac{r}{R_B} + \frac{1}{4} \frac{R_B}{r} \right] \right. \\ \left. Re_B \left[ \frac{R_B^2}{r^2} - \frac{R_B}{r} + \frac{r}{R_B} - 1 \right] \right\} \end{aligned} \quad [3.44]$$

We observe that [3.44] reduces to the result cited in Flint and Howarth (9), for the case of Stokes' flow, with  $St = 0$ ,  $G \neq 0$ , when  $Re_B^* = 0$ ; however,  $Re_B^* = 0 \Leftrightarrow Re_B = 0$  is precisely the condition under which the intermediate flow of Yoon and Luttrell (4) reduces to Stokes flow around the bubble.

We now employ  $\Psi^{int}$ , as given by [3.44], to compute  $P_c$  for an intermediate flow around the bubble when  $St = 0$  and  $G \neq 0$ . The grazing trajectory generated by the particle path stream function in [3.44] satisfies

$$\Psi^{int}(r, \theta) = \text{const.} \equiv \Psi^{int}\left(R_p + R_B, \frac{\pi}{2}\right) \quad [3.45]$$

or

$$\begin{aligned} \Psi^{int}(r, \theta) &= v_B R_B^2 \left\{ \left[ \frac{1}{2}(1 + |G|) \frac{(R_p + R_B)^2}{R_B^2} \right. \right. \\ &\quad \left. \left. - \frac{3}{4} \frac{R_p + R_B}{R_B} + \frac{1}{4} \frac{R_B}{R_p + R_B} \right] \right. \\ &\quad \left. + Re_B^* \left[ \frac{R_B^2}{(R_p + R_B)^2} - \frac{R_B}{R_p + R_B} + \frac{R_p + R_B}{R_B} - 1 \right] \right\} \\ &\equiv v_B \mathcal{J}(R_p, R_B; |G|, Re_B^*) \end{aligned} \quad [3.46]$$

where  $\mathcal{J}(R_p, R_B; |G|, Re_B^*)$  has the obvious definition.

In [3.46] we now assume that  $r \geq r_c$  so that, by virtue of [3.22],  $\sin \theta = R_c/r$ ; by using this result in [3.44] to compute  $\Psi^{int}$  (for  $r \geq r_c$ ) and then substituting the resulting expression for the left-hand side of [3.46] we obtain, after some simplification,

$$\begin{aligned} R_c^2 &\left\{ \left[ \frac{1}{2}(1 + |G|) - \frac{3}{4} \frac{R_B}{r} + \frac{1}{4} \frac{R_B^3}{r^3} \right] \right. \\ &\quad \left. + Re_B^* \left[ \frac{R_B^4}{r^4} - \frac{R_B^3}{r^3} + \frac{R_B}{r} - \frac{R_B^2}{r^2} \right] \right\} \\ &= \mathcal{J}(R_p, R_B; |G|, Re_B^*) \end{aligned} \quad [3.47]$$

Letting  $r \rightarrow \infty$  in [3.47] yields

$$\frac{1}{2}(1 + |G|)R_c^2 = \mathcal{J}(R_p, R_B; |G|, Re_B^*)$$

or, by virtue of the definition of  $\mathcal{J}$  which is implied by [3.46]

$$R_c^2 = \frac{1}{1+|G|} \left\{ \left[ (R_p + R_B)^2(1+|G|) - \frac{3}{2}R_B(R_p + R_B) + \frac{1}{2} \frac{R_B^3}{R_p + R_B} \right] + 2Re_B^* \left[ \frac{R_B^4}{(R_p + R_B)^2} - \frac{R_B^3}{R_p + R_B} + R_B(R_p + R_B) - R_B^2 \right] \right\} \quad [3.48]$$

Therefore, as an exact expression for  $P_c$  in this case we obtain (recall that

$$P_c = R_c^2 / (R_B + R_p)^2) :$$

$$P_c^{int} = \frac{1}{1+|G|} \left\{ \left[ (1+|G|) - \frac{3}{2} \frac{R_B}{R_p + R_B} + \frac{1}{2} \frac{R_B^3}{(R_p + R_B)^3} \right] + 2Re_B^* \left[ \frac{R_B^4}{(R_p + R_B)^4} - \frac{R_B^3}{(R_p + R_B)^3} + \frac{R_B}{R_p + R_B} - \frac{R_B^2}{(R_p + R_B)^2} \right] \right\} \quad [3.49]$$

It is easily determined that the second [ ] on the right-hand side of [3.49] reduces to

$$\frac{1}{(R_p + R_B)^4} \{ R_B R_p^3 + 2R_B^2 R_p^2 \} \quad [3.50a]$$

while elementary algebraic manipulations yield

$$\begin{aligned} (1+|G|) - \frac{3}{2} \frac{R_B}{R_p + R_B} + \frac{1}{2} \frac{R_B^3}{(R_p + R_B)^3} \\ = \frac{1}{2(R_p + R_B)^3} \{ 2R_p^3 + 3R_p^2 R_B \\ + 2|G|(R_p^3 + R_B^3) + 6|G|(R_p^2 R_B + R_B^2 R_p) \} \end{aligned} \quad [3.50b]$$

Combining the last two results above with [3.49] yields

$$\begin{aligned} (1+|G|)P_c^{int} &= \frac{1}{2(R_p + R_B)^3} \{ 2R_p^3 + 3R_p^2 R_B + 2|G|(R_p^3 + R_B^3) \\ &\quad + 6|G|(R_p^2 R_B + R_B^2 R_p) \} \\ &\quad + \frac{2Re_B^*}{(R_p + R_B)^4} \{ R_B R_p^3 + 2R_B^2 R_p^2 \} \end{aligned}$$

or

$$P_c^{int} = \frac{1}{1+|G|} \left[ \frac{1}{2(R_p + R_B)^3} \{ 2R_p^3 + 3R_p^2 R_B \} + \frac{2Re_B^*}{(R_p + R_B)^4} \{ R_B R_p^3 + 2R_B^2 R_p^2 \} \right] + \frac{|G|}{1+|G|} \quad [3.51]$$

**Remarks:** For intermediate flow, in the sense of Yoon and Luttrell (4), with the particle settling velocity assumed to be negligible, we may set  $G = 0$  in [3.51] so as to obtain

$$\begin{aligned} \hat{P}_c^{int} = & \frac{1}{2(R_p + R_B)^3} \{2R_p^3 + 3R_p^2 R_B\} \\ & + \frac{2Re_B^*}{(R_p + R_B)^4} \{R_B R_p^3 + 2R_B^2 R_p^2\} \end{aligned} \quad [3.52]$$

On the other hand, setting  $Re_B^* = 0 \Leftrightarrow Re_B = 0$  in [3.51] yields the exact collision probability for Stokes' flow around the bubble with  $St = 0, G \neq 0$ , i.e.

$$P_c^{st} = \frac{1}{1 + |G|} \left[ \frac{1}{2(R_p + R_B)^3} \{2R_p^3 + 3R_p^2 R_B\} \right] + \frac{|G|}{1 + |G|} \quad [3.53]$$

Finally, for Stokes' flow around the bubble with  $St = 0$  and  $G = 0$ , [3.53] yields

$$\hat{P}_c^{st} = \frac{1}{2(R_p + R_B)^3} \{2R_p^3 + 3R_p^2 R_B\} \quad [3.54]$$

**Remarks:** The expressions [3.51], [3.52] for intermediate flow and [3.53], [3.54] for Stokes flow around the bubble are *exact relations* which depend only on the hypotheses that  $St \approx 0$  and that the fluid flow streamlines are symmetric fore and aft of the bubble so that the collision angle  $\theta_c = \pi/2$  (in both [3.52] and [3.54] we also assume that  $G \approx 0$ ). To the best of the authors' knowledge, the *exact* expressions in [3.51]-[3.54] have not appeared previously in the literature. What has appeared in the literature are approximate relations for  $P_c^{int}$ ,  $\hat{P}_c^{int}$ ,  $P_c^{st}$ , and  $\hat{P}_c^{st}$  which depend on certain additional assumptions concerning the magnitudes  $R_p$  and  $R_B$  that have never been clearly delineated in the literature; these are summarized below.

**Remarks:** From [3.51] and [3.53] we obtain the so-called limiting 'efficiencies'

$$E_c^{int} = \lim_{R_p \rightarrow 0} P_c^{int} \equiv \frac{|G|}{1 + |G|} \quad [3.55a]$$

and

$$E_c^{st} = \lim_{R_p \rightarrow 0} P_c^{st} \equiv \frac{|G|}{1 + |G|} \quad [3.55b]$$

The result in [3.55b] has appeared in Flint and Howarth (9). The result in [3.55b] follows from an approximate relation for  $P_c^{int}$  which is listed in Table 1 of Nguyen-Van (11). The authors have been unable to find a derivation of the approximate relation for  $P_c^{int}$  which is cited in (11); thus, this relation is derived below as a direct consequence of the exact expression [3.51].

The most familiar approximate relation in the literature is the one for  $\hat{P}_c^{st}$ , which we indicate below. Actually the oldest form of approximate relation is that for  $\hat{P}_c^{pot}$ ,  $\hat{P}_c^{pot} = 3\left(\frac{R_p}{R_B}\right)$ , which was first given by Sutherland (3), where ‘pot’ denotes potential flow around the bubble and ^ indicates that  $G \approx 0$ , as well as  $St \approx 0$ ; because the results for potential flow do not follow directly as a special case of those for intermediate flow, the derivations of the exact and approximate results for  $P_c^{pot}$  and  $\hat{P}_c^{pot}$  are given, for the sake of completeness, in Appendices A and B.

To initiate the delineation of the various approximate results, we assume in [3.54] that

$$R_p + R_B \simeq R_B \quad [3.56]$$

and

$$\left(\frac{R_p}{R_B}\right)^3 \ll \left(\frac{R_p}{R_B}\right)^2 \quad [3.57]$$

In this case, we obtain from [3.54]

$$\hat{P}_c^{st} \simeq \left(\frac{3}{2}\right) \frac{R_p^2}{R_B^2} \quad [3.58]$$

a well-known result that has been often cited, e.g. Schulze (8), but never clearly identified as an approximate relationship; the same degree of approximation as that indicated in both

[3.56] and [3.57] allows one to conclude, as a consequence of [3.53], that

$$P_c^{st} \simeq \frac{3}{2(1+|G|)} \left( \frac{R_p^2}{R_B^2} \right) + \frac{|G|}{1+|G|} \quad [3.59]$$

The result in [3.59] appears as the first entry of Table 1 in Nguyen-Van (11) but a derivation of this (albeit) approximate result does not appear in the reference cited there, i.e., in Gaudin (26). Turning to the exact expression for  $P_c^{int}$ , i.e., [3.51] we now assume the validity of both [3.57] and [3.58] and, thus, deduce that

$$P_c^{int} \simeq \frac{1}{1+|G|} \left[ \left( \frac{3}{2} + 4Re_B^* \right) \frac{R_p^2}{R_B^2} \right] + \frac{|G|}{1+|G|} \quad [3.60]$$

The (approximate) result in [3.60] appears as the fourth entry in Table 1 of Nguyen-Van (11) but does not appear in the references cited there, e.g., in Yoon and Luttrell (4); what does appear in (4), albeit without a derivation, is the approximate result for  $\hat{P}_c^{int}$  which follows either from [3.60] by setting  $G = 0$ , i.e.,

$$\hat{P}_c^{int} = \left( \frac{3}{2} + 4Re_B^* \right) \frac{R_p^2}{R_B^2} \quad [3.61]$$

or from the exact result [3.52] by employing the assumptions [3.56] and [3.57].

### 3.2 $P_c$ Predictions

The exact intermediate flow solution for  $P_c$  [3.51] may be rearranged to yield

$$P_c^{int} = \frac{1}{1+|G|} \left\{ \frac{1}{2 \left[ \left( \frac{R_p}{R_B} \right) + 1 \right]^3} \left[ 2 \left( \frac{R_p}{R_B} \right)^3 + 3 \left( \frac{R_p}{R_B} \right)^2 \right] + \frac{2Re_B^*}{\left[ \left( \frac{R_p}{R_B} \right) + 1 \right]^4} \left[ \left( \frac{R_p}{R_B} \right)^3 + 2 \left( \frac{R_p}{R_B} \right)^2 \right] \right\} + \frac{|G|}{1+|G|} \quad [3.62]$$

with  $Re_B^* = Re_B^{0.72}/15$ . Therefore, the three dimensionless groups of  $R_p/R_B$ ,  $|G|$ , and  $Re_B$  are the only parameters that influence the probability of collision. The expression [3.62] will be used in this section to identify significant ranges of these dimensionless groups that influence  $P_c$ . These results will first be presented by fixing the dimensionless particle settling velocity,  $|G|$ , varying  $R_p/R_B$ , and performing calculations for selected values of  $Re_B$ . The bubble Reynolds number,  $Re_B$ , will then be held constant and calculations will be performed for selected values of  $|G|$  over the range of  $R_p/R_B$ . The particle/bubble radius ratio will then be fixed to present various predictions. Comparisons will also be made between the model presented here and experimental data available from the mineral flotation industry for  $P_c$ .

### 3.2.1 Fixed $|G|$ Predictions

The nondimensional parameter  $|G| (= |v_{ps}/v_B|)$  is the magnitude of the dimensionless settling velocity. Many authors have developed approximations for  $P_c$  assuming  $|G| = 0$ ; the three most common referenced flows include potential flow [7.14] (3), Stokes flow [3.58] (8), and the intermediate flow of Yoon and Luttrell [3.61] (4). In addition to assuming  $|G| = 0$  in these approximations, additional assumptions are invoked (i.e., [3.56] and [3.57]). Figure 4 reveals these three common approximations for  $P_c$  as a function of  $R_p/R_B$ . Stokes flow [3.58] corresponds to the intermediate flow of Yoon and Luttrell (4) when  $Re_B = 0$  and this flow predicts the lowest value for  $P_c$  for all  $R_p/R_B \leq 1$ , with  $P_c$  increasing as  $R_p/R_B$  increases. The values of  $P_c$  predicted for intermediate flow [3.61] are a function of  $Re_B$  and selected  $Re_B$  values are shown in Fig. 4 for  $Re_B \leq 500$ . The applicability of these results at  $Re_B = 500$  is questionable because they were developed for  $0 \leq Re_B \leq 100$ ; however, Yoon and Luttrell (4) state that it “may be applicable for  $Re_B > 100$ , although no experimental (streamline) data [were] available in the present work”. This figure also reveals that  $P_c$  increases as

$Re_B$  increases for a fixed ratio  $R_p/R_B$ , and these values run parallel to those predicted for Stokes flow. Potential flow predictions [7.14] are also shown in Fig. 4 for completeness. Potential flow predicts the highest values for  $P_c$  when  $R_p/R_B \lesssim 0.1$ , depending on  $Re_B$ . One interesting result from this figure is that all three flow conditions predict values for  $P_c > 1$  as  $R_p/R_B \rightarrow 1$ , revealing that assumption [3.56] is critical and must hold for these predictions to yield realistic results.

Assuming the intermediate flow stream function of Yoon and Luttrell (4) is valid and  $|G| = 0$ , but not introducing the simplifying assumptions [3.56] and [3.57], the exact intermediate flow result for  $P_c$  can be determined (i.e., [3.62]). This equation, along with the approximate solution of Yoon and Luttrell, is shown in Fig. 5 for  $Re_B \leq 500$ . The exact and approximate solutions follow closely to one another for small values of  $R_p/R_B$ , and at  $R_p/R_B = 0.1$ , the approximate solution presented by Yoon and Luttrell (4) overpredicts  $P_c$  by approximately 25% when  $Re_B = 0$  and by more than 35% when  $Re_B = 500$ . Increasing  $R_p/R_B$  further toward 1 increases this difference. By employing the flow of Yoon and Luttrell (4) in the development of the exact solution for  $P_c$  [3.62], the predictions are valid for  $Re_B \leq 100$ , but their utility is suspect for  $Re_B > 100$ . However, calculations are shown for  $Re_B = 500$  to reveal that the same trends are followed and unrealistic predictions ( $P_c > 1$ ) result only when  $R_p/R_B \gtrsim 0.3$  and  $Re_B = 500$ . This result will be further discussed below.

Figures 6-11 reveal the exact predictions for  $P_c$  [3.62] for a range of  $Re_B$  and fixed values of  $|G|$ . The exact value for Stokes flow [3.53] corresponds to  $Re_B = 0$  in these figures. All figures show that the bubble Reynolds number has a negligible effect on the  $P_c$  predictions when  $R_p/R_B \lesssim 0.05$ , and  $P_c$  is constant for a given value of  $|G|$ , with a higher constant value of  $P_c$  corresponding to larger values of  $|G|$ . When  $R_p/R_B \gtrsim 0.05$ ,  $P_c$  increases exponentially with increasing  $R_p/R_B$ . Additionally, the increase in  $P_c$  is more abrupt as  $Re_B$  increases. When

$R_p/R_B = 1$ ,  $P_c \leq 1$  for  $Re_B \leq 100$ . As previously stated, these predictions are questionable when  $Re_B > 100$  because the stream function used to generate [3.62] included data only up to  $Re_B = 100$  (4). In our predictions, when  $Re_B = 500$  and  $R_p/R_B \gtrsim 0.3$ ,  $P_c > 1$ , but  $P_c$  is independent of  $Re_B$  when  $R_p/R_B \lesssim 0.05$  and [3.51] or [3.62] can be used outside its given  $Re_B$  range under these specific conditions.

### 3.2.2 Fixed $Re_B$ Predictions

Calculations similar to those presented above have been completed using [3.62] for fixed  $Re_B$  over the given  $R_p/R_B$  range and for selected values of  $|G|$ . Figure 12 reveals one such plot for  $Re_B = 0$ , which corresponds to Stokes flow conditions. This figure represents the exact Stokes flow solution [3.53]. The approximate Stokes flow result often cited in the literature, [3.58], is identical to the approximate intermediate flow solution of Yoon and Luttrell (4) with  $Re_B = 0$  and  $|G| = 0$ , and is also shown here for reference.

In general,  $P_c$  increases with increasing  $|G|$ ; Fig. 12 shows that for small  $R_p/R_B$ ,  $|G|$  has a significant effect on the  $P_c$  predictions and the effect diminishes at large  $R_p/R_B$ . When  $R_p/R_B$  is small,  $P_c$  increases with increasing  $|G|$  by several orders of magnitude when compared to the  $|G| = 0$  predictions, implying the particle settling velocity significantly enhances the collision probability when collision occurs between a particle that is much smaller than the colliding bubble. This would be particularly true for particles with a density much larger than that of water. The increase in  $P_c$  with increasing  $|G|$  is much smaller when a particle and bubble are the same order of magnitude (with  $R_p < R_B$ ), and as  $R_p/R_B \rightarrow 1$ ,  $P_c$  predictions approach the same value independent of  $|G|$ . In Fig. 12, all  $P_c$  predictions are less than 1 for  $R_p/R_B \leq 1$ , except, for reasons previously stated, the approximate solution of Yoon and Luttrell (4).

Figures 13-18 show similar trends for other fixed  $Re_B$  values. The approximate solution of Yoon and Luttrell (4) (applicable for  $|G| = 0$ ) is also shown in each figure as a reference. When  $Re_B \leq 100$  (Figs. 12-17), the exact predictions [3.62] reveal  $P_c \leq 1$  for  $R_p/R_B \leq 1$ . Additionally, as  $Re_B$  increases (Fig. 12 to Fig. 18), it is evident that  $P_c$  becomes independent of  $|G|$  as  $R_p/R_B \rightarrow 1$ . When  $Re_B = 500$  (Fig. 18), unrealistic results occur when  $R_p/R_B \gtrsim 0.3$  because the Yoon and Luttrell (4) stream function employed in this  $P_c$  derivation is outside its range of applicability. However, these  $P_c$  predictions are valid for  $R_p/R_B \lesssim 0.05$  because, as discussed in Section 3.2.1,  $P_c$  is independent of  $Re_B$  in this region.

Applying assumptions [3.56] and [3.57] to the exact result for  $P_c$  [3.51] yields [3.60], which is the result found in Yoon and Luttrell (4) with the inclusion of the particle settling velocity ( $|G|$ ). Figures 19-21 compare these approximations to the exact result for  $Re_B = 0, 10,$  and  $100$ , respectively. Again, the Yoon and Luttrell (4) result ( $|G| = 0$ ) is shown in each figure as a reference. The approximate  $P_c$  predictions [3.60] and the exact  $P_c$  predictions [3.51] are equivalent for small  $R_p/R_B$ . When  $R_p/R_B \approx 0.03, 0.05,$  and  $0.2$ , the approximate solution begins to deviate from the exact solution when  $|G| = 0, 0.01,$  and  $1$ , respectively, and  $Re_B = 0$  (Fig. 19). The deviation between the exact and approximate solution occurs at slightly smaller  $R_p/R_B$  ratios as  $Re_B$  increases (Figs. 20 and 21). Also, as  $R_p/R_B$  increases, the approximate solution asymptotes to the Yoon and Luttrell (4) solution [3.61], which does not include the effects of particle settling velocity. These figures reveal that particle settling velocity is important at small values of  $R_p/R_B$  and assumptions [3.56] and [3.57] are not. Conversely, as  $R_p/R_B \rightarrow 1$ , assumptions [3.56] and [3.57] dominate and the inclusion of  $|G|$  has only a secondary effect (and only at low bubble Reynolds numbers).

### 3.2.3 Fixed $R_p/R_B$ Predictions

Additional calculations have been performed for fixed values of  $R_p/R_B$  when both  $|G|$  and  $Re_B$  are varied. These predictions result in contour plots of  $P_c$  for each fixed value of  $R_p/R_B$  (Figs. 22-26).

When  $R_p/R_B = 0.01$  (Fig. 22), the contour lines are plotted with logarithmic increments, showing that  $P_c$  varies over two orders of magnitude for the given conditions. For  $R_p/R_B = 0.01$ ,  $P_c$  is a strong function of  $|G|$  but is independent of  $Re_B$ . Increasing  $R_p/R_B$  to 0.05 (Fig. 23), reveals that  $P_c$  is still independent of  $Re_B$ , but only when  $|G| \gtrsim 0.05$ . When  $R_p/R_B = 0.1$  (Fig. 24),  $P_c$  is independent of  $Re_B$  only when  $|G| \gtrsim 0.2$ .

At  $R_p/R_B = 0.5$  (Fig. 25),  $P_c$  contours are now plotted on a linear scale with major divisions (solid lines) corresponding to  $P_c$  values in increments of 0.1 and minor divisions (dashed lines) representing  $P_c$  values in increments of 0.05. Under these conditions,  $P_c$  is independent of  $Re_B$  only for small  $Re_B$  and large  $|G|$ . Conversely,  $P_c$  is independent of  $|G|$  when  $|G|$  is small and  $Re_B$  is large. This trend continues when  $R_p/R_B = 0.9$  (Fig. 26). Therefore, as discussed earlier, when  $R_p/R_B$  is large, particle settling velocity only plays a minor role and only when  $Re_B$  is small and  $|G|$  is large.

### 3.2.4 Comparisons with Published Data

Direct experimental observations of the collision process are very complicated because it is difficult to isolate this microprocess from the other microprocesses in actual flotation separation. However, attempts to experimentally record  $P_c$  have been made by a few researchers addressing mineral flotation (4, 5, 10, 11, 16, 17). We will attempt to compare our predictions for  $P_c$  with this available experimental data.

For these comparisons, considerable effort was made to match the experimental conditions

as closely as possible. Specific parameters of importance were the bubble rise velocity and the particle and fluid thermophysical properties. It was assumed that all experiments were performed in a fluid with properties corresponding to those of water. In all cases, the particular particles used in the experiments were identified by name, but when the density was not provided, a value was chosen based on available tabulated data. The most difficult parameter to match was the bubble rise velocity because this parameter was not always provided for each experimental condition.

Predictions were first compared with experimental data presented by Anfruns and Kitchener (16, 17). They experimentally studied the probability of collision as a single bubble rose through a dilute suspension of quartz particles with a measured size distribution. Five quartz size fractions were used with mean diameters of 12.0, 18.0, 24.6, 31.4, and 40.5  $\mu\text{m}$ . These particle diameters and a quartz density of 2.65  $\text{g}/\text{cm}^3$ , obtained from Nguyen-Van and Kmet (10), were used in our calculations. The bubble rise velocity was obtained from data presented in (17) in which experimental results for  $v_B$  were presented in terms of bubble diameter. The data were obtained in two separate tubes with different diameters (0.5 and 3.3 cm). The experimental bubble rise velocity results are replotted in Fig. 27, which also includes the relationship

$$v_B = -2.72d_B^3 + 3.46d_B^2 + 9.64d_B \quad [3.63]$$

where  $d_B$  is the bubble diameter in mm and  $v_B$  is the bubble rise velocity in cm/s. This relationship was obtained by us using a polynomial curve fit to the experimental data.

Figure 28 displays  $P_c$  predictions made with [3.51] incorporating the above experimental information, and compares the predictions to the experimental data presented by Anfruns and Kitchener (16, 17). In all cases, the calculations overpredict the experimental data.

This is probably due to the experiments not sufficiently isolating  $P_c$ . In fact, Anfruns and Kitchener actually plot data as “Efficiency of Collection ( $E_c$ ),” which implies that it may also include adhesion by sliding ( $P_{asl}$ ) and stability ( $P_{stab}$ ) effects. Since the overall collection efficiency would be the product of each microprocess efficiency, the fact that the experimental data is below the  $P_c$  predictions is not surprising. This discrepancy was highlighted by Nguyen-Van and Kmet (10) in which they state: “In our opinion, the experimental results done by these authors [Anfruns and Kitchener] refer rather to [a] collection efficiency than to [a] collision one.”

Yoon and Luttrell (4, 5) also present mineral particle flotation data in which  $P_c$  predictions are also made. The experimental set up in these experiments was similar to Anfruns and Kitchener (16, 17); however, they utilized very hydrophobic Buller seam coal particles with 0.13% ash content and mean diameters of 11.4, 31.0, and 40.1  $\mu m$  in their experiments. According to Yoon and Luttrell (4), the probability of collection they recorded should closely match  $P_c$  since  $P_{asl}$  for very hydrophobic particles should approach unity. The density of individual coal particles is difficult to determine and it is a function, among other things, of the ash content (27). Yoon and Luttrell did not present any density values, so we used a value of 1.4 g/cm<sup>3</sup>, determined from Gray and MacKnight (27) for Buller seam coal with an ash content of 0.13%.

For their experimental facility, Yoon and Luttrell (28) state that the bubble rise velocity has the form

$$v_B = B(d_B^{1.14}) \quad [3.64]$$

where  $B$  is a proportionality constant obtained for a given set of experimental conditions. The constant was not provided, but was estimated by backing it out of  $Re_B$  which was

obtained from their  $P_c$  predictions and experimental conditions. The value of  $B$  employed in our calculations was  $B \approx 0.00462$ . In [3.64],  $d_B$  and  $v_B$  have units of  $\mu m$  and  $cm/s$ , respectively.

Figure 29 compares our  $P_c$  predictions to the results of Yoon and Luttrell (4, 5). Their predictions are also included in Fig. 29. Our predictions do very well at predicting  $P_c$ , particularly for the smaller particle diameters of 11.4 and 31.0  $\mu m$ . At  $d_p = 40.1 \mu m$ , [3.51] underpredicts the data slightly. This may be due to our estimates of  $\rho_p$  and  $v_B$  used in the calculations. However, the general trends are followed closely for all particle diameters considered. Our predictions do not differ significantly from those of Yoon and Luttrell (i.e., [3.61]) because for these conditions,  $R_p \ll R_B$  and  $|G|$  is on the order of 0.01 (or less).

Nguyen-Van (11) also presented  $P_c$  experimental data for two different particle types; galena ( $\rho_p = 7.5 \text{ g/cm}^3$ ,  $R_p = 6.25 \mu m$ ) and quartz ( $\rho_p = 2.65 \text{ g/cm}^3$ ,  $R_p = 7.75 \mu m$ ). Property data were obtained from Nguyen-Van and Kmet (10). These experiments involved a fixed bubble held in place on a capillary tube with fluid flowing past the bubble. A dilute particle suspension was injected above the bubble from a second (movable) capillary tube and was entrained in the moving fluid. Particle collisions with the fixed bubble were visually observed. This method allowed for  $R_c$  (see Fig. 1) to be experimentally determined. Since the bubble was fixed in these experiments, the bubble rise velocity was equivalent to the fluid velocity flowing past the bubble. The bubble rise velocity was obtained indirectly through  $Re_B$  from the following relationship

$$R_B = \left[ \frac{9\mu_l^2 Re_B (1 + 0.15 Re_B^{0.687})}{4\rho_l^2 g} \right]^{1/3} \quad [3.65]$$

which was presented in (10) and claimed to agree with experimental data.

Figure 30 presents the quartz data from Nguyen-Van (11). Nguyen-Van also developed

a prediction for  $P_c$ , and this is also plotted in the figure. This prediction included the possibility that the maximum collision angle may be less than  $90^\circ$  from the stagnation point on the bubble. This prediction has the form

$$P_c = \frac{1}{1 + |G|} \left( \frac{R_p}{R_B} \right)^2 \left[ \frac{\sqrt{(X + C)^2 + 3Y^2} - (X + C)}{13.5Y^2} \right] \left[ \sqrt{(X + C)^2 + 3Y^2} + 2(X + C) \right]^2 \quad [3.66]$$

where

$$C = \frac{2R_B^2 \Delta \rho g}{9\mu_\ell v_B} \quad [3.67]$$

$$X = 1.5 \left[ 1 + \frac{3Re_B/16}{1 + 0.309Re_B^{0.694}} \right] \quad [3.68]$$

$$Y = \frac{3Re_B/8}{1 + 0.217Re_B^{0.518}} \quad [3.69]$$

One can easily see that this  $P_c$  prediction is rather complicated, but the Nguyen-Van  $P_c$  prediction follows the experimental data very closely. Our  $P_c$  prediction [3.51] has a much simpler form and also does a good job of following the data. The largest discrepancy is at the largest  $R_B$  values, but this is still within  $\sim 25\%$  of the experimental data. This deviation between our predictions and the experimental data may be due to the collision angle having an effect at these conditions. The inclusion of assumptions [3.56] and [3.57] yields [3.60], which is also shown in Fig. 30. This result does not significantly differ from that of [3.51] because the experimental conditions satisfy the assumptions incorporated into the approximation. The predictions of Yoon and Luttrell (4) [3.61] are also shown in Fig. 30 and do not predict the experimental results very well, indicating that  $|G|$  has a significant effect for these experimental conditions.

Figure 31 reveals the same type of comparisons, but for the galena data of Nguyen-Van (11). Galena has a much higher density than that of quartz, so particle settling velocity would be much more significant. This is evident by the fact that the Yoon and Luttrell (4) predictions significantly underpredict the experimental data. Our current  $P_c$  predictions [3.51] and [3.60] (with the associated assumptions) do a very good job of predicting the experimentally determined  $P_c$  values. The more complicated  $P_c$  prediction of Nguyen-Van also does a very good job.

In summary, our model for the probability of collision does a very good job of predicting available experimental results for  $P_c$ . The model is less complicated than that proposed by Nguyen-Van (11), but just as accurate, and is much improved over the model of Yoon and Luttrell (4).

## 4 Conclusions

In this report, we developed an exact solution for  $P_c$  (i.e., [3.51]) based on the intermediate flow field of Yoon and Luttrell (4). This solution includes the effects of particle settling velocity and only assumes that the bubble and particle are spherical and that  $R_p < R_B$  (we do not require that  $R_p \ll R_B$ ). These results were used to predict  $P_c$  for  $0 \leq Re_B \leq 500$ ,  $0 \leq |G| \leq 5$ , and  $0.001 \leq R_p/R_B \leq 1$ .

In general,  $P_c$  is independent of  $Re_B$  when  $R_p/R_B \lesssim 0.05$  for all values of  $|G|$ . Conversely,  $P_c$  is not significantly influenced by  $|G|$  as  $R_p/R_B \rightarrow 1$  for all values of  $Re_B$ . Simplifying assumptions [3.56] and [3.57], which are typically employed in the literature, are valid only when  $R_p/R_B \lesssim 0.05 - 0.1$ .

Finally, the new model expressions for  $P_c$  presented here do a good job of predicting the available experimental data. The inclusion of the particle settling velocity is very important,

particularly when the particles have a density much higher than that of water. Additionally, the form of  $P_c$  derived from basic principles in this report is much simpler than that proposed by Nguyen-Van (11), and just as accurate at predicting experimental results.

## 5 References

1. Heindel, T.J. and Bloom, F., **Mathematical Modelling of the Overall Flotation Deinking Process**, Rep. 1, Project F00903, IPST, Atlanta, Ga., 1995.
2. Heindel, T.J. and Bloom, F., **Mathematical Modelling of the Overall Flotation Deinking Process: Predictions of Selected Performance Parameters**, Rep. 2, Project F00903, IPST, Atlanta, Ga., 1996.
3. Sutherland, K.L., "Physical Chemistry of Flotation XI. Kinetics of the Flotation Process", **J. Phys. Chem.**, **52**, 1947, 394-425.
4. Yoon, R.H. and Luttrell, G.H., "The Effect of Bubble Size on Fine Particle Flotation", in **Mineral Processing and Extractive Metallurgy Review**, **5**, 1989, 101-122.
5. Luttrell, G.H. and Yoon, R.H., "A Hydrodynamic Model for Bubble-Particle Attachment", **J. Colloid and Interface Sci.**, **154**, 1992, 129-137.
6. Ahmed, N. and Jameson, G.J., "Flotation Kinetics", in **Mineral Processing and Extractive Metallurgy Review**, **5**, 1989, 77-99.
7. Schulze, H.J., "Flotation as a Heterocoagulation Process: Possibilities of Calculating the Probability of Flotation", in **Coagulation and Flocculation**, B. Dobias, ed., 1993, 321-353.
8. Schulze, H.J., **Physicochemical Elementary Processes in Flotation**, Elsevier, Amsterdam, 1984.
9. Flint, L.R. and Howarth, W.J., "The Collision Efficiency of Small Particles with Spherical Air Bubbles", **Chem. Eng. Sci.**, **26**, 1971, 1155-1168.
10. Nguyen-Van, A. and Kmet, S., "Collision Efficiency for Fine Mineral Particles with a Single Bubble in a Countercurrent Flow Regime", **Int. J. Mineral Processing**, **35**, 1992, 205-223.
11. Nguyen-Van, A., "The Collision between Fine Particles and Single Air Bubbles in Flotation", **J. Colloid and Interface Sci.**, **162**, 1994, 123-128.
12. Weber, M.E., "Collision Efficiencies for Small Particles with a Spherical Collector at Intermediate Reynolds Numbers", **J. Separ. Proc. Technol.**, **2**, 1981, 29-33.
13. Weber, M.E. and Paddock, "Interceptional and Gravitational Collision Efficiencies for Single Collectors at Intermediate Reynolds Numbers", **J. Colloid and Interface Sci.**, **94**, 1983, 328-335.

14. Reay, D. and Ratcliff, G.A., "Removal of Fine Particles from Water by Dispersed Air Flotation: Effects of Bubble Size and Particle Size on Collision Efficiency", **The Canad. J. Chem. Eng.**, **51**, 1973, 178-185.
15. Dobby, G.S. and Finch, J.A., "Particle Size Dependence in Flotation Derived from a Fundamental Model of the Capture Process", **Int. J. Min. Process**, **21**, 1987, 241-260.
16. Anfruns, J.P. and Kitchener, J.A., "Rate of Capture of Small Particles in Flotation", **Trans. Inst. Min. Metall., Sect. C.**, **86**, 1977, C9-C15.
17. Anfruns, J.P. and Kitchener, J.A., "The Absolute Rate of Capture of Single Particles by Single Bubbles", in **Flotation**, M. Fuerstenau, ed., A.M. Gaudin Memorial Volume, **2**, AIME, N.Y., 1976, 625-637.
18. Spielman, L.A., "Particle Capture from Low-Speed Laminar Flows", **Ann. Rev. Fluid Mech.**, **9**, 1977, 297-319.
19. Michael, D.H. and Norey, P.W., "Particle Collision Efficiencies for a Sphere", **J. Fluid Mech.**, **37**, 1969, 565-575.
20. Bloom, F. and Heindel, T.J., "Mathematical Modelling of the Flotation Deinking Process", **Mathl. Comput. Modelling**, **25**, 1997, 13-58.
21. Heindel, T.J. and Bloom, F., "New Measures for Maximizing Ink Particle Removal in a Flotation Cell", in the **Proc. 1997 TAPPI Recycling Symp.**, 101-113.
22. Bloom, F. and Heindel, T.J., "A Theoretical Model of Flotation Deinking Efficiency", **J. Colloid and Interface Sci.**, **190**, 1997, 182-197.
23. Matis, K.A. and Zouboulis, A.I., "The Role of Bubble/Particle Size", in **Flotation Science and Engineering**, K.A. Matis, ed., Marcel Dekker, Pub. N.Y., 1995.
24. Cheremisinoff, M.P., "Industrial Sedimentation Practices", Chp 16 of the **Encyclopedia of Fluid Mechanics, 5: Slurry Flow Technology**, N.P. Cheremisinoff, ed., 1986, 686-717.
25. Batchelor, G.K., **An Introduction to Fluid Dynamics**, Cambridge Univ. Press, 1990.
26. Gaudin, A.M., **Flotation**, 2nd ed., McGraw-Hill, N.Y., 1957.
27. Gray, V.R. and MacKnight, F.J., "The Apparent Relative Density of New Zealand Coals" **New Zealand Journal of Geology and Geophysics**, **29**, 1986, 463-470.
28. Yoon, R.H. and Luttrell, G.H., "The Effect of Bubble Size on Fine Coal Flotation," **Coal Preparation**, **2**, 1986, 179-192.

## 6 Nomenclature

- $Ar$  - Archimedes number
- $C_D$  - coefficient of drag (for a particle)
- $C_D^{st}$  - coefficient of drag in Stokes flow
- $d_p$  - particle diameter
- $d_B$  - bubble diameter
- $E_c^{int}$  - limiting efficiency in intermediate flow  
 $\left( \lim_{R_p \rightarrow 0} P_c^{int} \right)$
- $E_c^{pot}$  - limiting efficiency in potential flow  
 $\left( \lim_{R_p \rightarrow 0} P_c^{pot} \right)$
- $E_c^{st}$  - limiting efficiency in Stokes flow  $\left( \lim_{R_p \rightarrow 0} P_c^{st} \right)$
- $F_b$  - magnitude of the buoyancy force acting on a particle
- $F_{dx}$  -  $x$  component of the drag force on a particle
- $F_{dy}$  -  $y$  component of the drag force on a particle
- $F_g$  - magnitude of the gravitational force acting on a particle
- $\mathbf{F}_d$  - drag force acting on a particle
- $f$  - friction factor
- $f(\theta)$  - arbitrary function of the angular coordinate
- $G$  - dimensionless particle settling velocity  $\left( = \lambda \frac{\tilde{v}_{ps}}{v_B} \equiv \frac{v_{ps}}{v_B} \right)$
- $g$  - acceleration due to gravity
- $h(r)$  - arbitrary function of the radial coordinate
- $m$  - inertial particle mass
- $\tilde{P}_c$  - probability of collision as given in (17)

- $P_c$  - microprocess probability of capture of a particle by a bubble
- $P_c^{int}$  - probability of collision in intermediate flow
- $\hat{P}_c^{int}$  -  $P_c^{int}$  at  $G = 0$
- $P_c^{pot}$  - probability of collision in potential flow
- $\bar{P}_c^{pot}$  - probability of collision in potential flow as given in (11)
- $\hat{P}_c^{pot}$  -  $P_c^{pot}$  at  $G = 0$
- $\tilde{P}_c^{pot}$  - probability of collision for potential flow based on the result for  $P_c$  as given in (17), i.e., based on  $\tilde{P}_c$
- $P_c^{st}$  - probability of collision in Stokes flow
- $\hat{P}_c^{st}$  -  $P_c^{st}$  at  $G = 0$
- $R_B$  - bubble radius
- $R_c$  - limiting capture radius of a streaming tube
- $Re_p$  - particle Reynolds number
- $Re_B$  - bubble Reynolds number
- $Re_B^*$  -  $\left(\frac{1}{15} Re_B^{0.72}\right)$
- $R_p$  - particle radius
- $r$  - radial distance of a particle from a bubble
- $r_c$  - smallest value of  $r$  such that for all  $r \geq r_c$  a particle approaching a bubble will be at the distance  $R_c$  from the stagnation line through the center of the bubble
- $r^*$  - dimensionless radial distance ( $r/R_B$ )
- $St$  - Stokes number
- $\mathcal{J}$  -  $\left(R_c^2 \left\{ \left[ \frac{1}{2}(1+G) - \frac{3R_B}{4r} + \frac{1}{4} \frac{R_B^3}{r^3} \right] + Re_B^* \left[ \frac{R_B^4}{r^4} - \frac{R_B^3}{r^3} + \frac{R_B}{r} - \frac{R_B^2}{r^2} \right] \right\} \right)$
- $t$  - time
- $t^*$  - dimensionless time ( $tv_B/R_B$ )

$\mathbf{u}$	-	fluid velocity
$\mathbf{u}^*$	-	dimensionless fluid velocity ( $\mathbf{u}/v_B$ )
$u_r$	-	radial component of the fluid velocity
$u_r^{int}$	-	radial component of the fluid velocity in an intermediate flow
$u_r^*$	-	radial component of the dimensionless fluid velocity
$u_x$	-	$x$ component of the fluid velocity field
$u_y$	-	$y$ component of the fluid velocity field
$u_x^*$	-	dimensionless $x$ -component of the fluid velocity
$u_y^*$	-	dimensionless $y$ -component of the fluid velocity
$u_\theta$	-	angular component of the fluid velocity
$u_\theta^{int}$	-	angular component of the fluid velocity in an intermediate flow
$u_\theta^*$	-	angular component of the dimensionless fluid velocity
$\mathbf{v}_p$	-	particle velocity
$\mathbf{v}_p^*$	-	dimensionless particle velocity ( $\mathbf{v}_p/v_B$ )
$v_{pr}$	-	radial component of the particle velocity
$v_{pr}^*$	-	radial component of the dimensionless particle velocity
$\mathbf{v}_{ps}$	-	particle settling velocity
$v_{ps}$	-	magnitude of the particle settling velocity
$\tilde{v}_{ps}$	-	magnitude of the particle settling velocity in Stokes flow
$v_{px}$	-	$x$ component of the particle velocity
$v_{py}$	-	$y$ component of the particle velocity
$v_{px}^*$	-	dimensionless $x$ -component of the particle velocity
$v_{py}^*$	-	dimensionless $y$ -component of the particle velocity
$v_{p\theta}$	-	angular component of the particle velocity

- $v_{p\theta}^*$  - angular component of the dimensionless particle velocity  
 $v_B$  - bubble rise velocity  
 $\hat{\alpha}$  -  $\left(1 - \frac{4}{3}Re_B^* \left(1 - \frac{1}{r^*}\right)\right)$   
 $\Delta\rho$  -  $(\rho_p - \rho_\ell)$   
 $\lambda$  - dimensionless friction factor  $(6\pi\mu_\ell R_p/f)$   
 $\mu_\ell$  - fluid viscosity  
 $\nu_\ell$  - kinematic fluid viscosity  
 $\Psi$  - particle stream function  
 $\Psi^{int}$  - particle stream function in intermediate flow  
 $\Psi^*$  - dimensionless particle stream function  
 $\Psi^{*int}$  - dimensionless particle stream function in intermediate flow  
 $\Psi^{*pot}$  - dimensionless particle stream function in potential flow  
 $\psi^{*int}$  - dimensionless stream function for intermediate flow  
 $\psi^{int}$  - stream function for intermediate flow  
 $\psi^{pot}$  - stream function for potential flow  
 $\psi^{st}$  - stream function for Stokes flow  
 $\rho_\ell$  - fluid density  
 $\rho_p$  - particle density  
 $\theta_c$  - collision angle  
 $\theta_0$  -  $\sin^{-1}(R_c/r_c)$

## 7 Appendices

### 7.1 Appendix A: Exact and Approximate Collision Probabilities for Potential Flow

For potential flow, with  $St \approx 0$ ,  $G \neq 0$ , the dimensionless particle path stream function has been given by Flint and Howarth (9) in the form

$$\Psi^{*pot} = \frac{1}{2} \sin^2 \theta \left\{ (1 + |G|) \frac{r^2}{R_B^2} - \frac{R_B}{r} \right\} \quad [7.1]$$

A grazing trajectory is, therefore, given by

$$\begin{aligned} \Psi^{*pot}(r, \theta) &= \Psi^{*pot} \left( R_p + R_B, \frac{\pi}{2} \right) \\ &\equiv \frac{1}{2} \left\{ (1 + |G|) \frac{(R_p + R_B)^2}{R_B^2} - \frac{R_B}{R_p + R_B} \right\} \end{aligned} \quad [7.2]$$

For  $r \geq r_c$ , we may substitute  $\sin \theta = \frac{R_c}{r}$  in [7.1] and the subsequent result on the left-hand side of [7.2]; this yields

$$R_c^2 \left\{ (1 + |G|) \frac{1}{R_B^2} - \frac{R_B}{r^3} \right\} = (1 + |G|) \frac{(R_p + R_B)^2}{R_B^2} - \frac{R_B}{R_p + R_B} \quad [7.3]$$

Letting  $r \rightarrow \infty$  in [7.3], and simplifying, we find that

$$R_c^2 = (R_p + R_B)^2 - \frac{1}{1 + |G|} \frac{R_B^3}{R_p + R_B}, \quad [7.4]$$

in which case, by virtue of [3.1],

$$P_c^{pot} = 1 - \frac{1}{1 + |G|} \frac{R_B^3}{(R_p + R_B)^3} \quad [7.5]$$

By algebraically combining the terms on the right-hand side of the exact relation [7.5] we obtain

$$P_c^{pot} = \frac{|G|}{1 + |G|} + \frac{1}{1 + |G|} \left[ \frac{3R_B^2 R_p + 3R_p^2 R_B + R_p^3}{(R_p + R_B)^3} \right] \quad [7.6]$$

The corresponding exact result for  $\hat{P}_c^{pot}$  may be obtained from [7.6] by setting  $G = 0$ ; for the limiting efficiency  $E_c^{pot}$  we again obtain

$$E_c^{pot} = \lim_{R_p \rightarrow 0} P_c^{pot} = \frac{|G|}{1 + |G|} \quad [7.7]$$

Under the auspices of the approximation [3.56] we obtain from [7.6]

$$P_c^{pot} \simeq \frac{|G|}{1 + |G|} + \frac{1}{1 + |G|} \left[ 3 \frac{R_p}{R_B} + 3 \frac{R_p^2}{R_B^2} + \frac{R_p^3}{R_B^3} \right] \quad [7.8]$$

Furthermore, if we also assume that [3.57] holds, then [7.8] reduces to

$$P_c^{pot} \simeq \frac{|G|}{1 + |G|} + \frac{3}{1 + |G|} \left[ \left( \frac{R_p}{R_B} \right) + \left( \frac{R_p}{R_B} \right)^2 \right] \quad [7.9]$$

Finally, if we strengthen [3.57] to

$$\left( \frac{R_p}{R_B} \right)^2 \ll \frac{R_p}{R_B} \quad [7.10]$$

then

$$P_c^{pot} \simeq \frac{|G|}{1 + |G|} + \frac{3}{1 + |G|} \left( \frac{R_p}{R_B} \right) \quad [7.11]$$

The result stated in [7.11] differs from that cited in Nguyen-Van (11), i.e.,

$$\bar{P}_c^{pot} = \frac{|G|}{1 + |G|} \left\{ 1 + \frac{R_p}{R_B} \right\}^2 + \frac{3}{1 + |G|} \left\{ \frac{R_p}{R_B} \right\} \quad [7.12]$$

In view of the structure of the exact result for  $P_c^{pot}$ , i.e., [7.5] or [7.6] it appears that [7.12] cannot be obtained as an approximation to  $P_c^{pot}$ . By expanding the first term on the right-hand side of [7.12], and employing [7.10], we obtain

$$\bar{P}_c^{pot} \simeq \frac{|G|}{1 + |G|} + \frac{3 + 2|G|}{1 + |G|} \left( \frac{R_p}{R_B} \right) \quad [7.13]$$

which conflicts with [7.11].

For  $G = 0$ , [7.11] reduces to the classical result first obtained by Sutherland (3), i.e.,

$$\hat{P}_c^{pot} \simeq 3 \left( \frac{R_p}{R_B} \right) \quad [7.14]$$

It is also true that both [7.12] and [7.13] reduce to the Sutherland (3) result, i.e., [7.14] when  $G = 0$ .

## 7.2 Appendix B: The Anfruns and Kitchener Results for $P_c$

In (16) and (17), Anfruns and Kitchener state a general result for  $P_c$  which applies to the case  $St \approx 0$ ,  $G \neq 0$ ; in our notation, this result assumes the form (see Anfruns and Kitchener, (17))

$$\tilde{P}_c = \frac{|G|}{1+|G|} \left( 1 + \frac{R_p}{R_B} \right)^2 + \frac{2}{1+|G|} \psi^* \left( R_p + R_B, \frac{\pi}{2} \right) \quad [7.15]$$

In particular, for potential flow around the bubble, with  $\psi^* = \psi^{*pot} \equiv \frac{1}{2} \sin^2 \theta \left( \frac{r^2}{R_B^2} - \frac{R_B}{r} \right)$ , [7.15] yields

$$\tilde{P}_c^{pot} = \frac{|G|}{1+|G|} \left( 1 + \frac{R_p}{R_B} \right)^2 + \frac{1}{1+|G|} \left\{ \frac{(R_p + R_B)^2}{R_B^2} - \frac{R_B}{R_p + R_B} \right\} \quad [7.16]$$

Combining, algebraically, the terms on the right-hand side of [7.16] we obtain

$$\tilde{P}_c^{pot} = \frac{|G|}{1+|G|} + \left( \frac{R_p}{R_B} \right)^2 + 2 \left( \frac{R_p}{R_B} \right) + \frac{1}{1+|G|} \frac{R_p}{R_p + R_B} \quad [7.17]$$

Using the same level of approximation as that which produced [7.11], namely, [3.56] and [7.10], we obtain from [7.17] the estimate

$$\tilde{P}_c^{pot} \simeq \frac{1}{1+|G|} + \left( 2 + \frac{1}{1+|G|} \right) \left( \frac{R_p}{R_B} \right) \quad [7.18]$$

Clearly [7.18] does not agree with [7.11]; however, [7.18] does reduce to the Sutherland (3) result [7.14] when  $G = 0$ .

It is also an easy exercise to show that the result cited in Nguyen-Van (11), i.e. [7.12], is an approximation to the Anfruns and Kitchener (16-17) result [7.16]; in fact if we combine the second grouping of terms on the right-hand side of [7.16] we easily find that

$$\begin{aligned} \tilde{P}_c^{pot} \simeq & \frac{1}{1+|G|} \left(1 + \frac{R_p}{R_B}\right)^2 \\ & + \frac{1}{1+|G|} \left\{ \left(\frac{R_p}{R_B}\right)^2 + \frac{2R_p^2 + 3R_p R_B}{R_B(R_p + R_B)} \right\} \end{aligned} \quad [7.19]$$

Using, first, the approximation  $R_p + R_B \simeq R_B$  in [7.19] produces

$$\begin{aligned} \tilde{P}_c^{pot} \simeq & \frac{|G|}{1+|G|} \left(1 + \frac{R_p}{R_B}\right)^2 \\ & + \frac{1}{1+|G|} \left\{ 3 \left(\frac{R_p}{R_B}\right)^2 + 3 \left(\frac{R_p}{R_B}\right) \right\} \end{aligned} \quad [7.20]$$

The additional approximation [7.10] then reduces [7.20] to [7.12], i.e., to the result cited in Table 1 of Nguyen-Van (11).

8 Figures

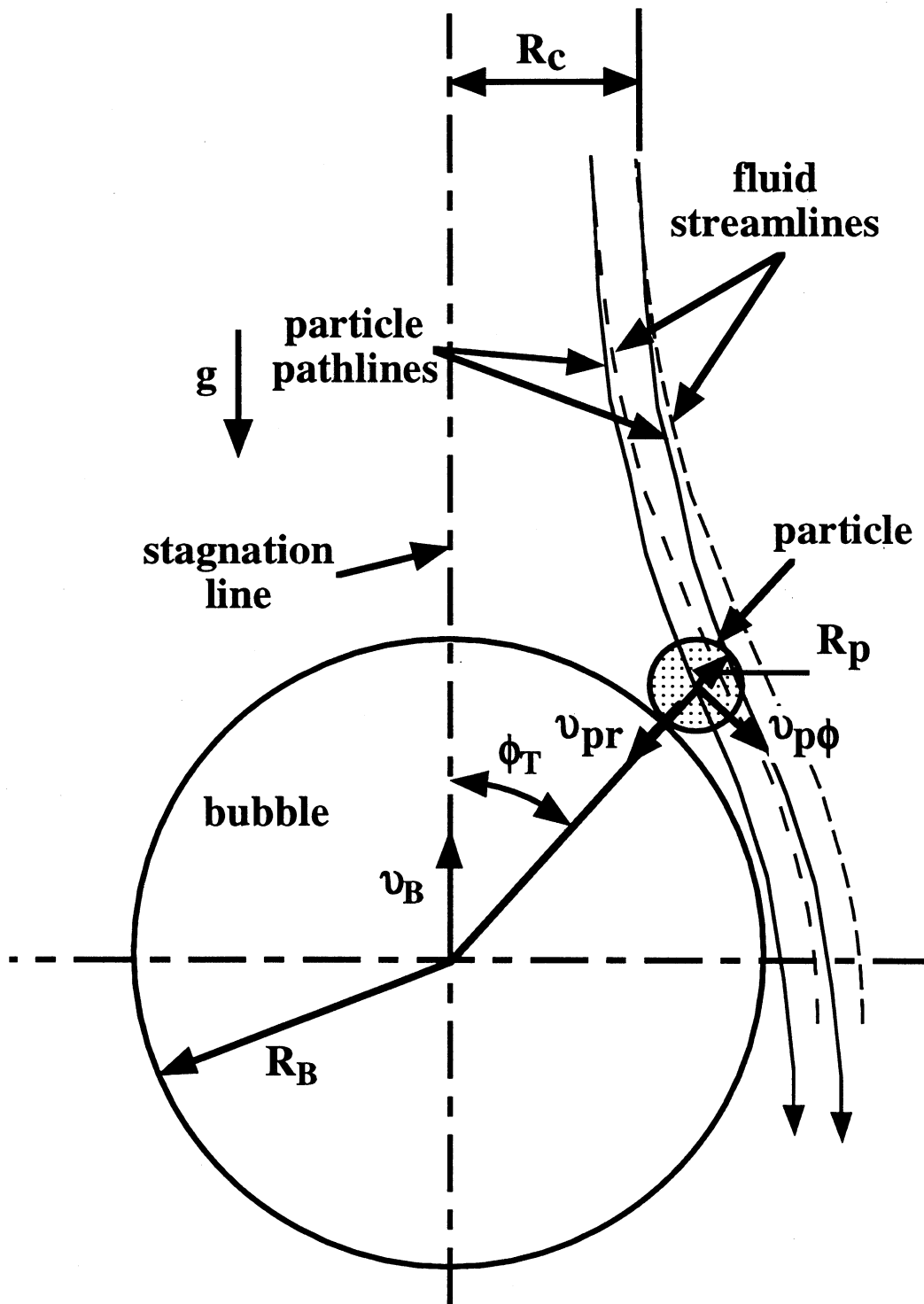


Figure 1: Particle approaching a bubble.

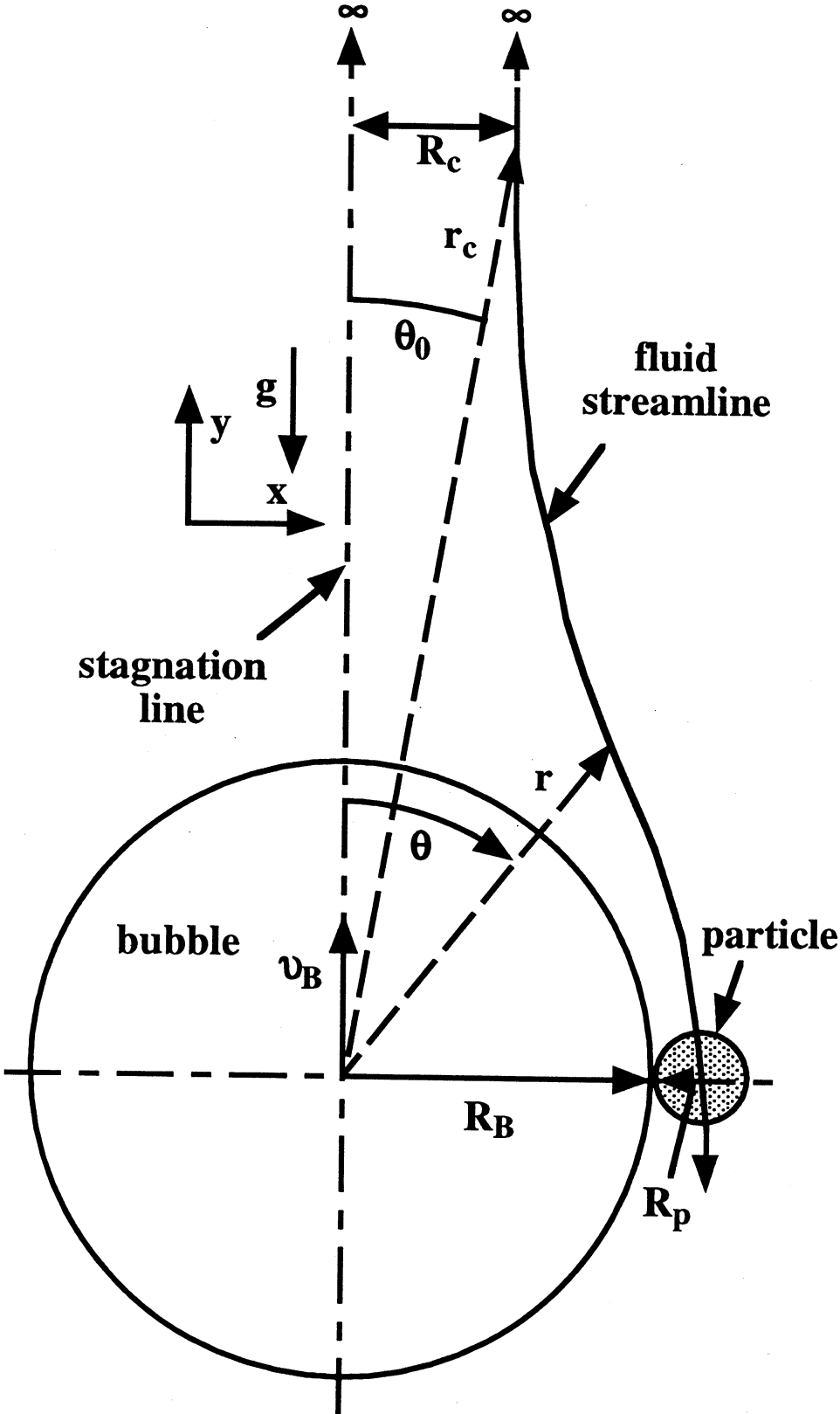


Figure 2: Particle colliding with a bubble at  $\theta_c = \pi/2$ .

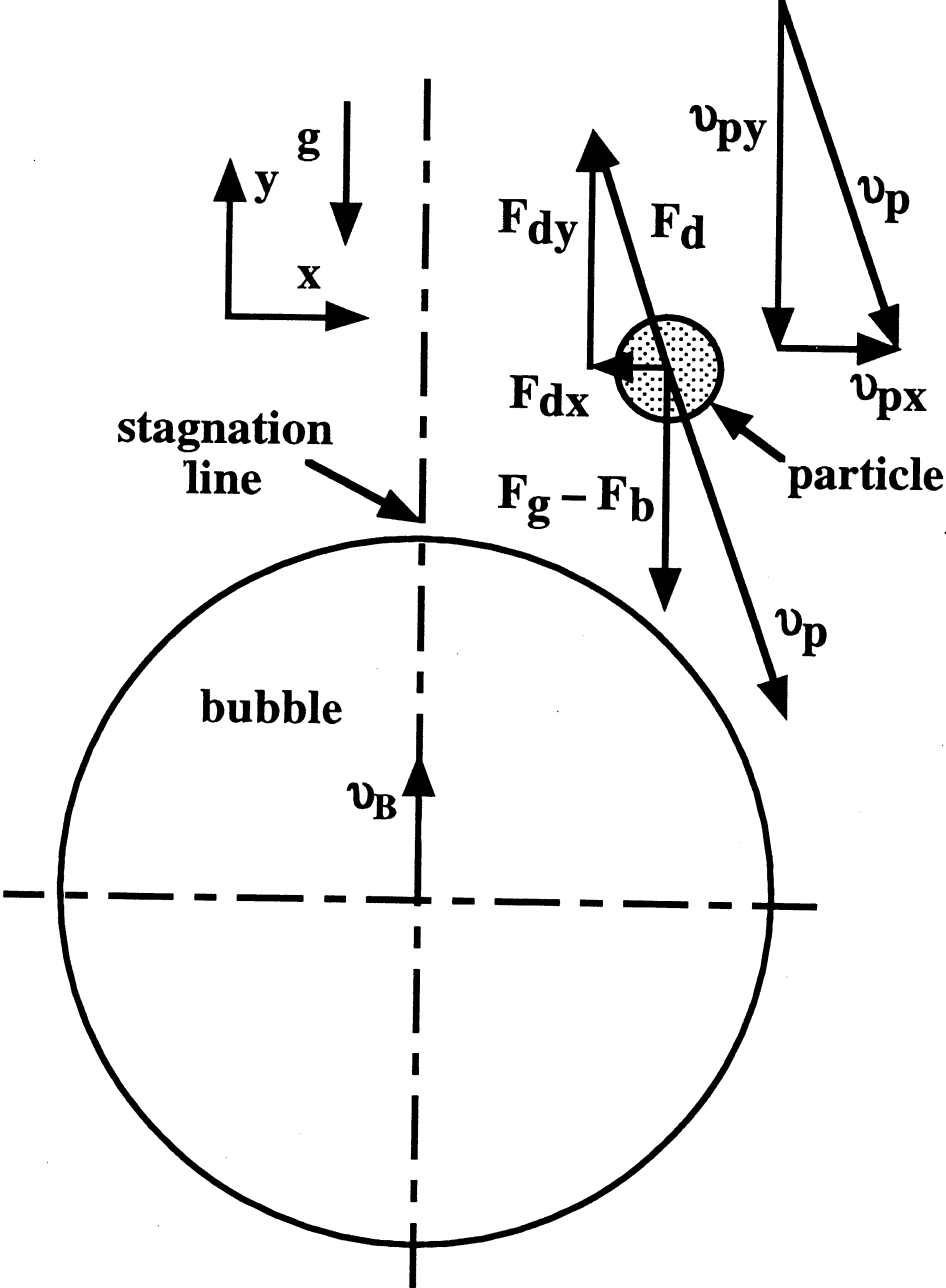


Figure 3: Forces acting on a particle as it approaches a bubble.

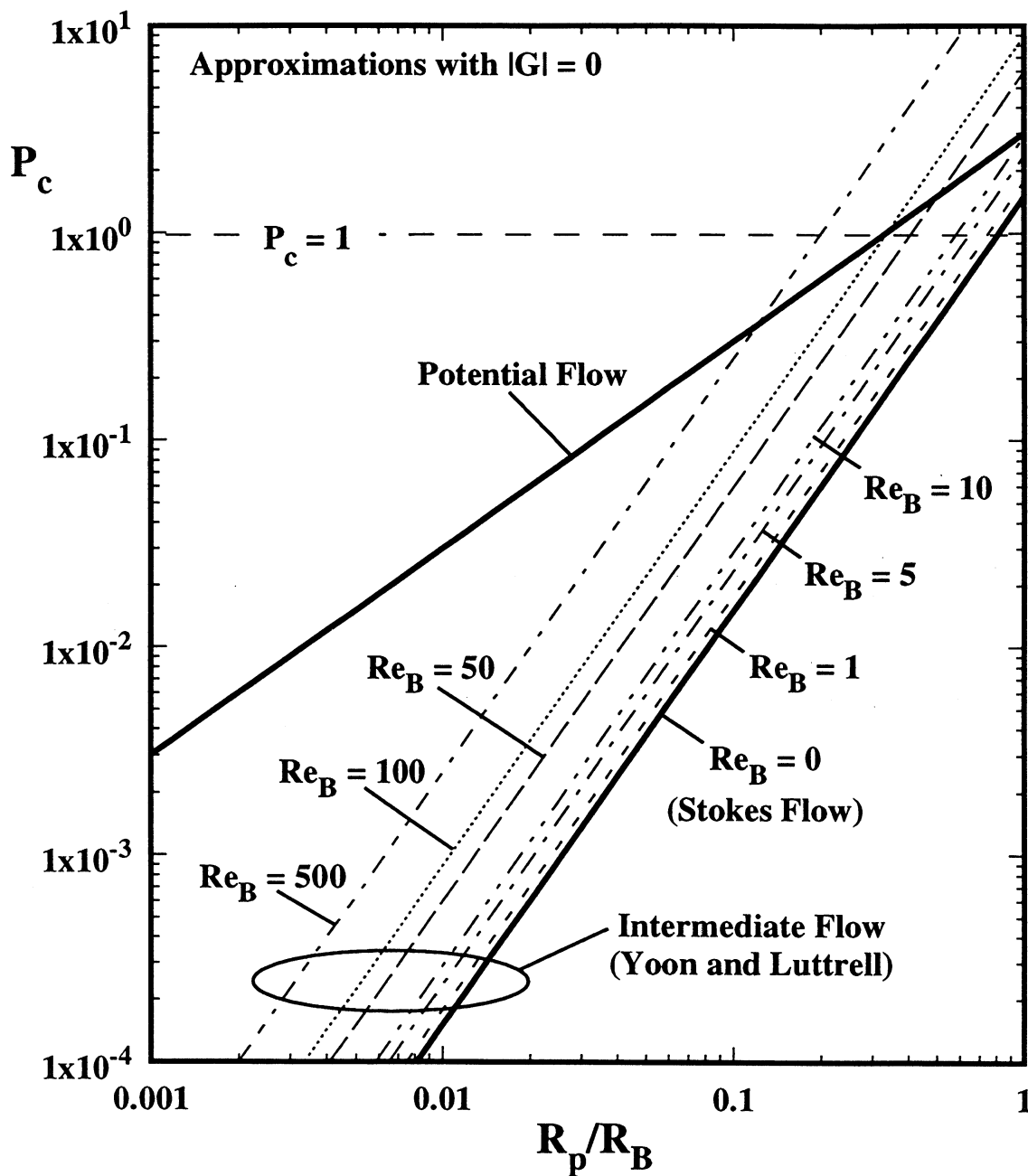


Figure 4: Probability of collision predictions based on potential flow [7.14], Stokes flow [3.58], and intermediate flow of Yoon and Luttrell [3.61].

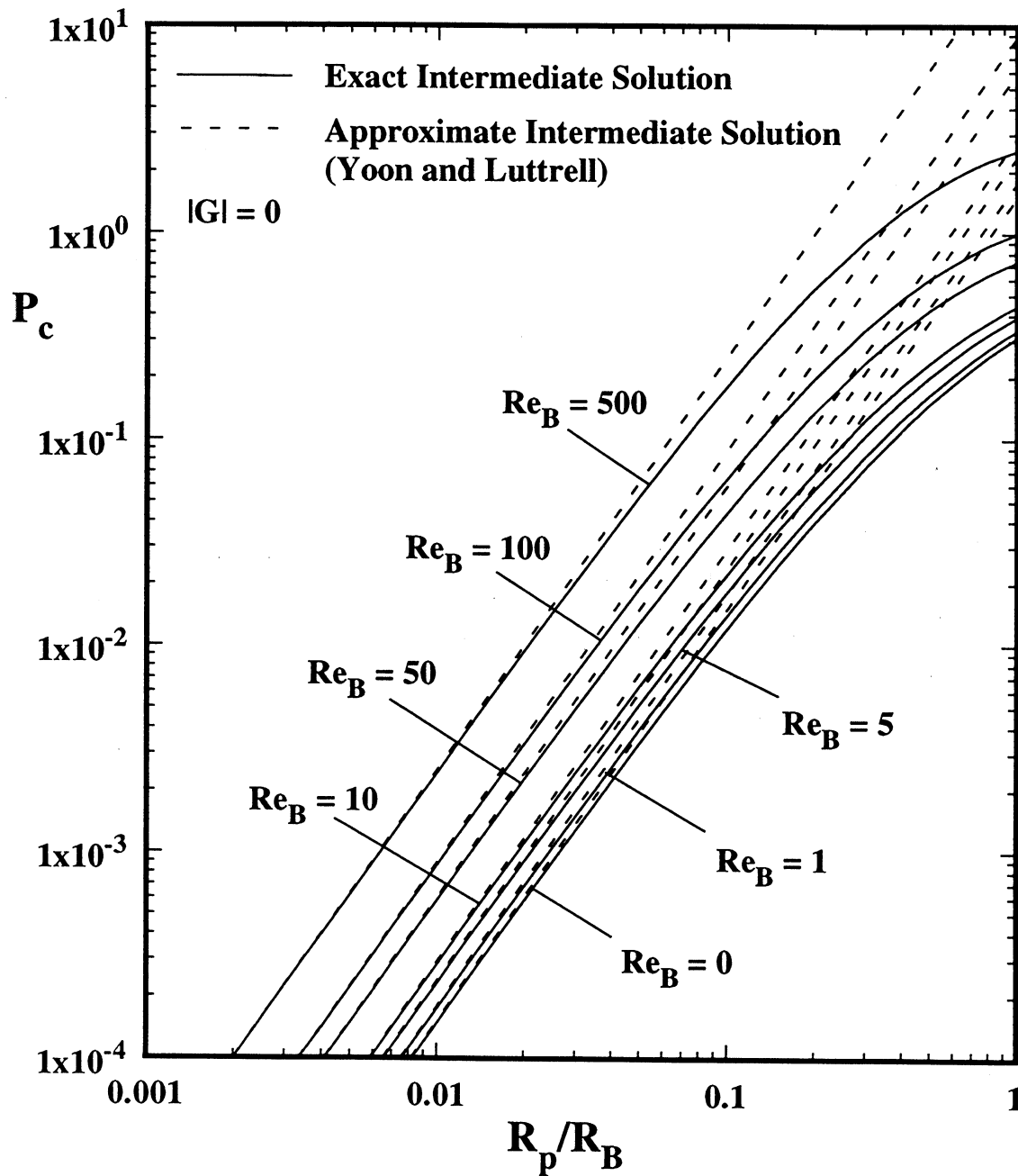


Figure 5: Exact and approximate  $P_c$  predictions for intermediate flow with  $0 \leq Re_B \leq 500$  and  $|G| = 0$ .

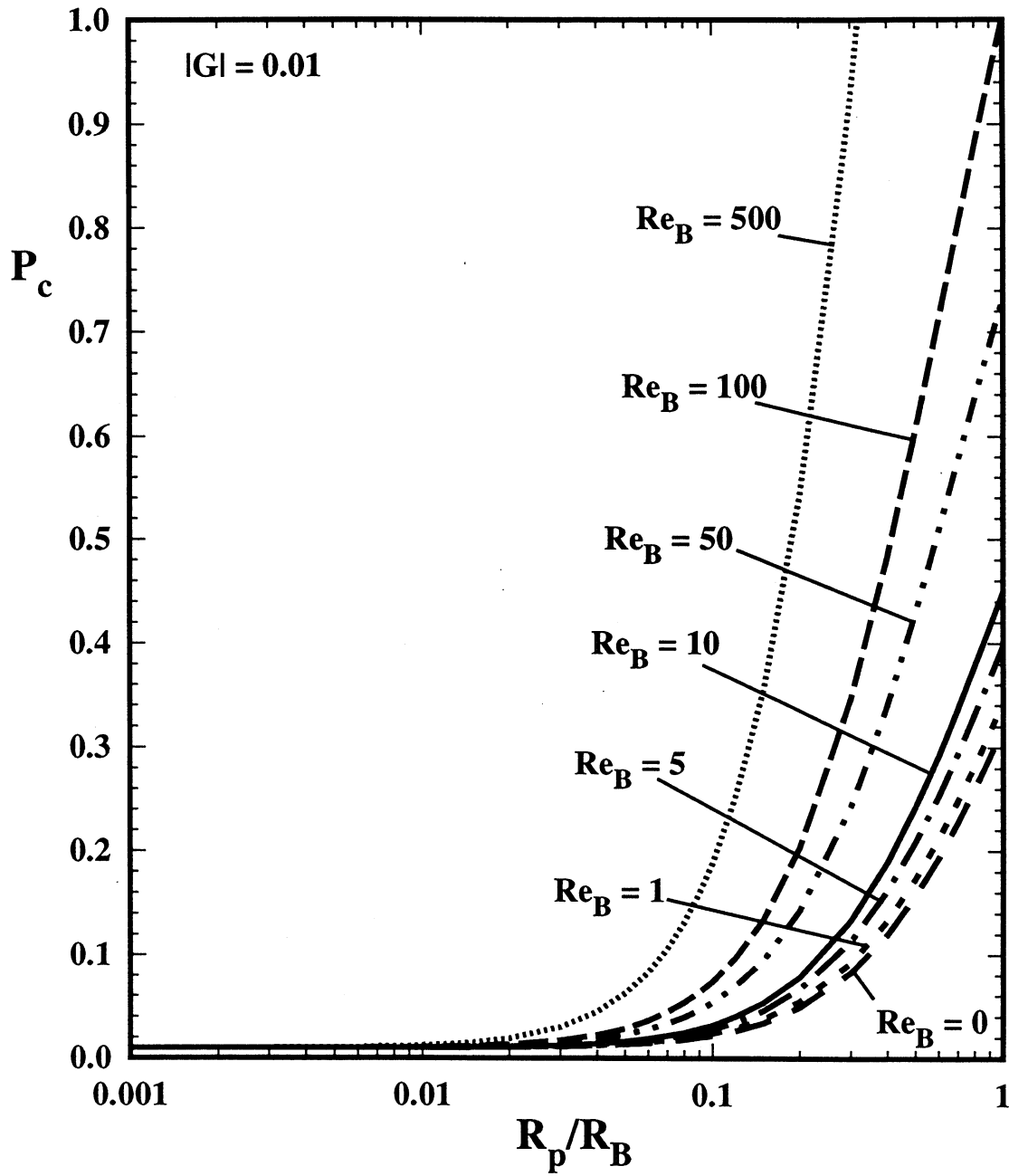


Figure 6: Exact  $P_c$  predictions for intermediate flow with  $0 \leq Re_B \leq 500$  and  $|G| = 0.01$ .

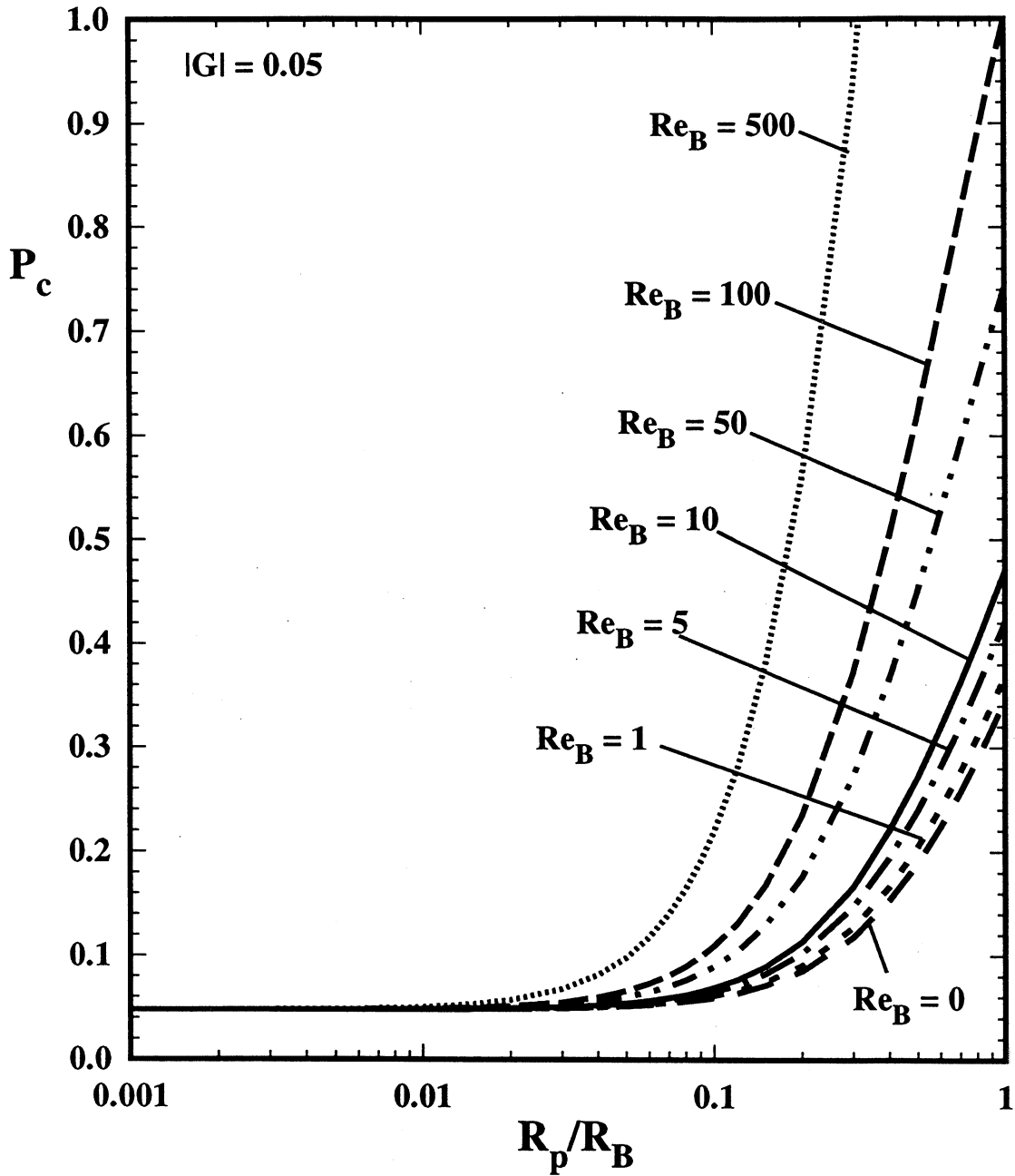


Figure 7: Exact  $P_c$  predictions for intermediate flow with  $0 \leq Re_B \leq 500$  and  $|G| = 0.05$ .

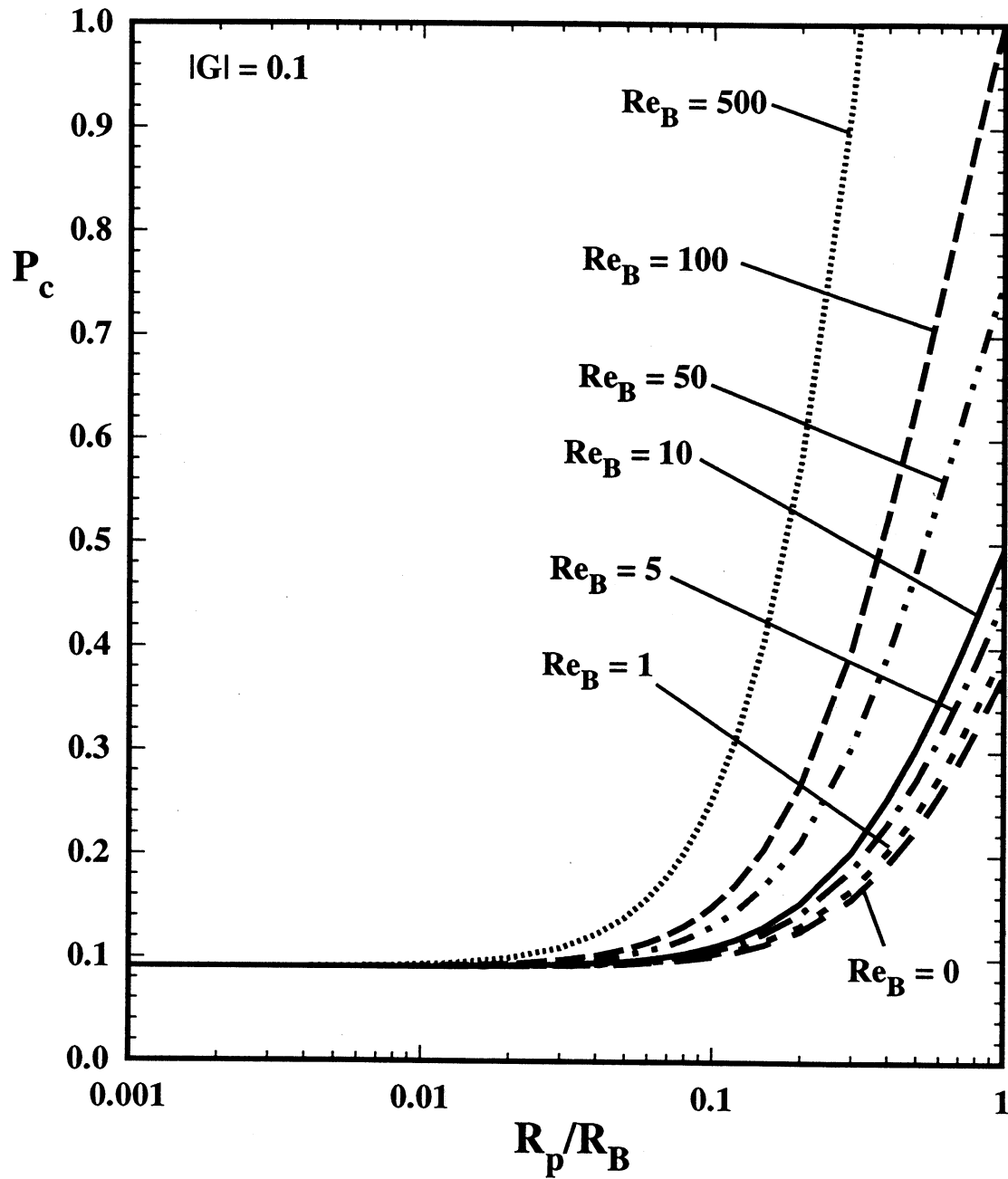


Figure 8: Exact  $P_c$  predictions for intermediate flow with  $0 \leq Re_B \leq 500$  and  $|G| = 0.1$ .

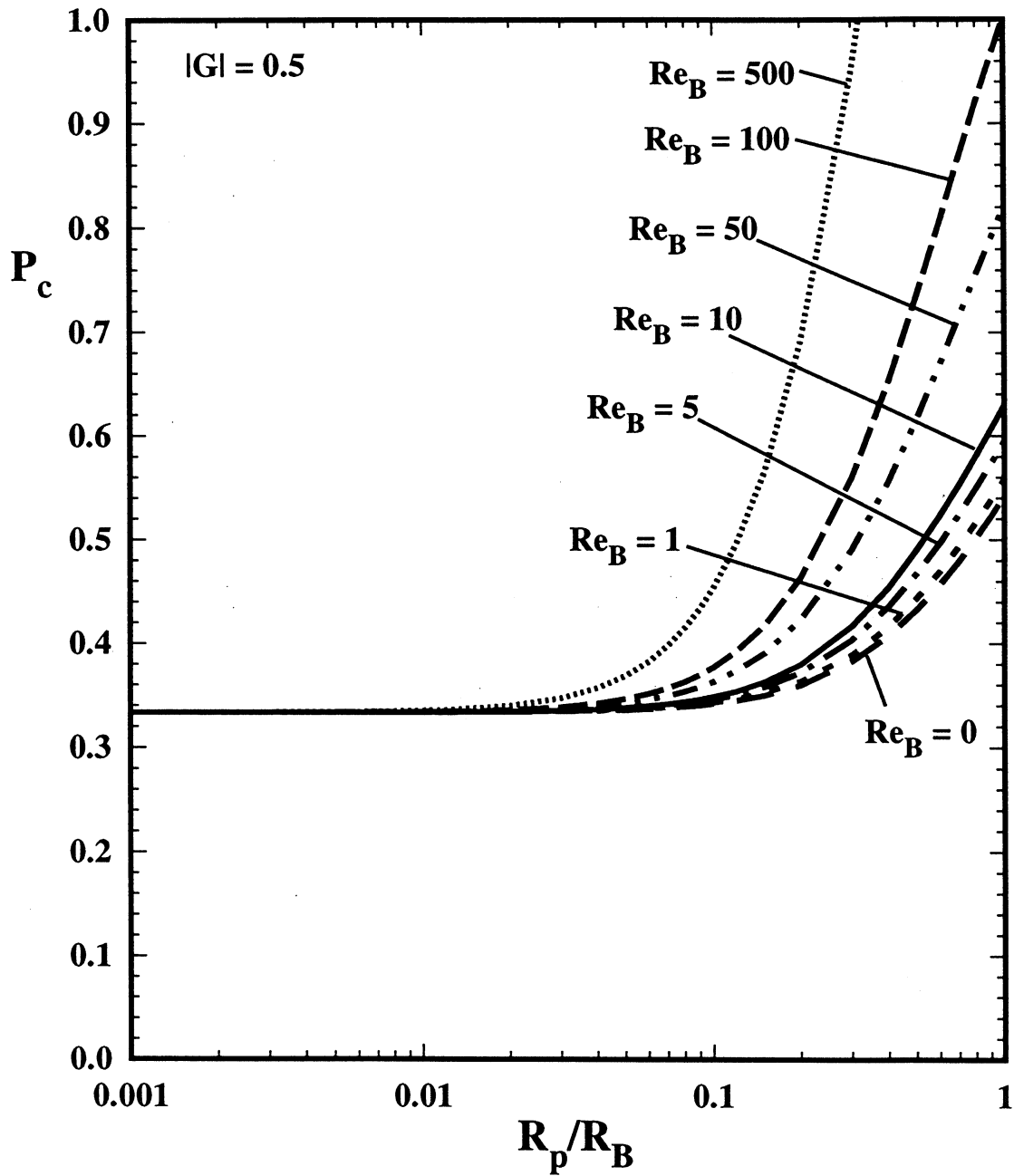


Figure 9: Exact  $P_c$  predictions for intermediate flow with  $0 \leq Re_B \leq 500$  and  $|G| = 0.5$ .

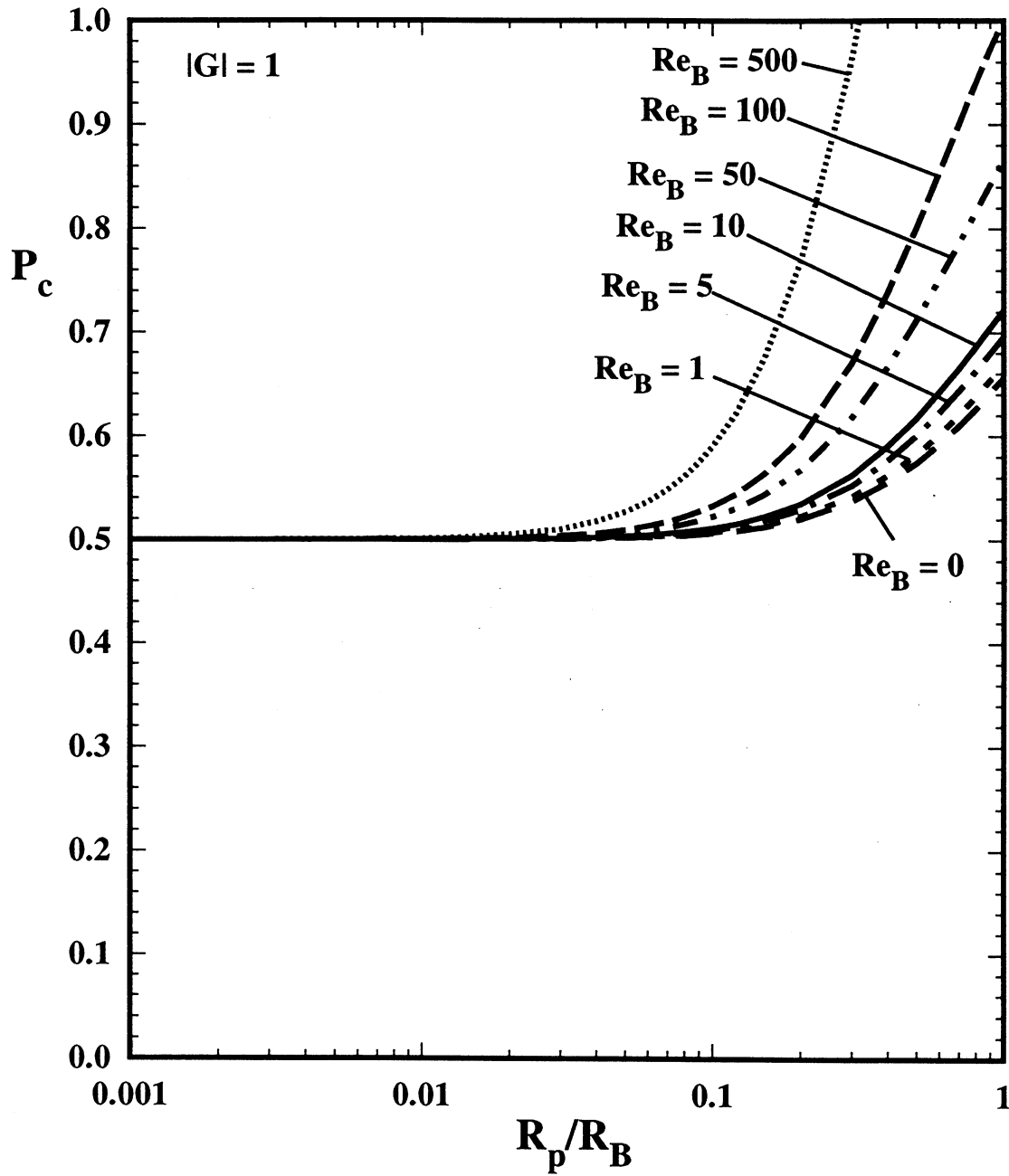


Figure 10: Exact  $P_c$  predictions for intermediate flow with  $0 \leq Re_B \leq 500$  and  $|G| = 1$ .

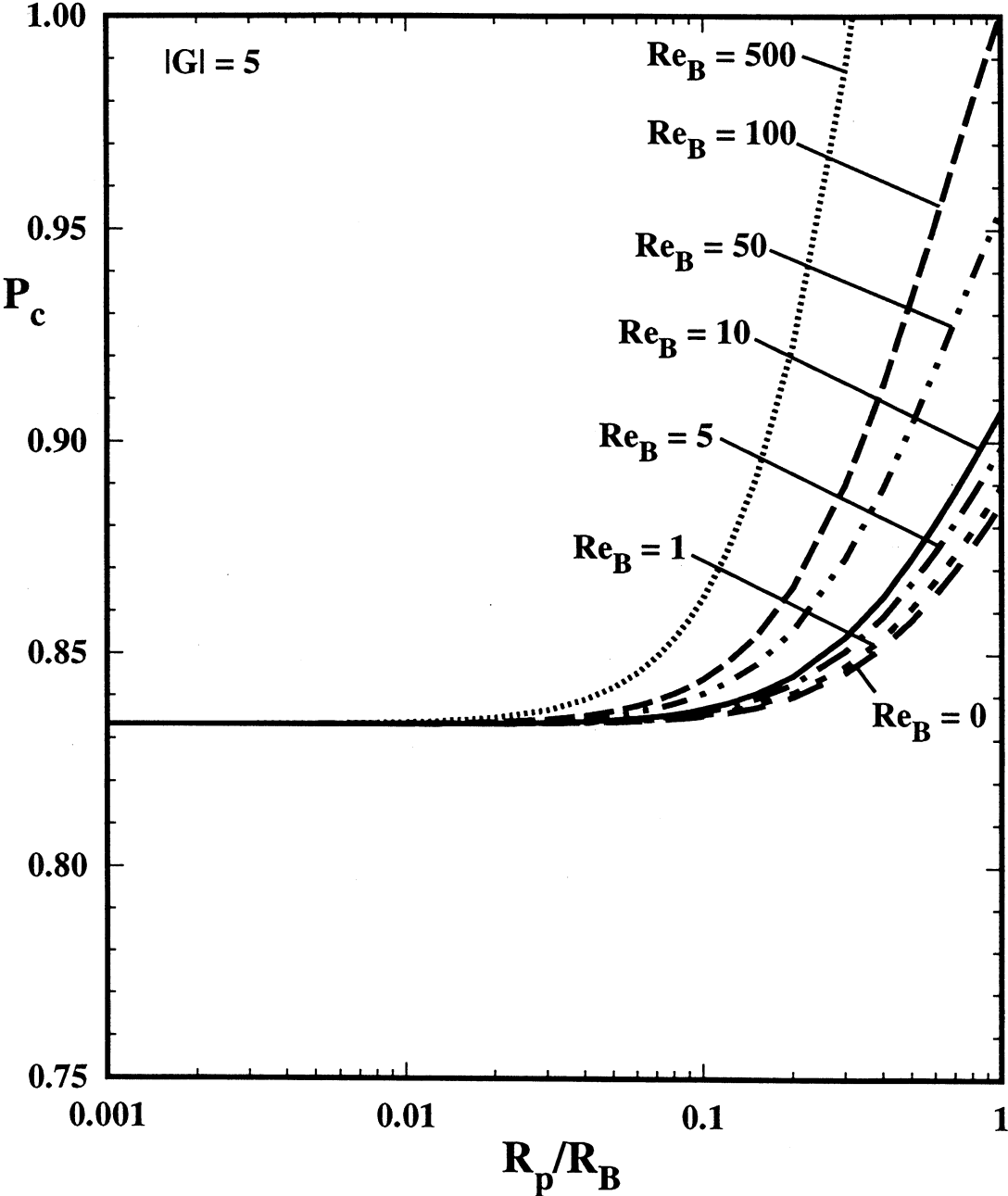


Figure 11: Exact  $P_c$  predictions for intermediate flow with  $0 \leq Re_B \leq 500$  and  $|G| = 5$ .

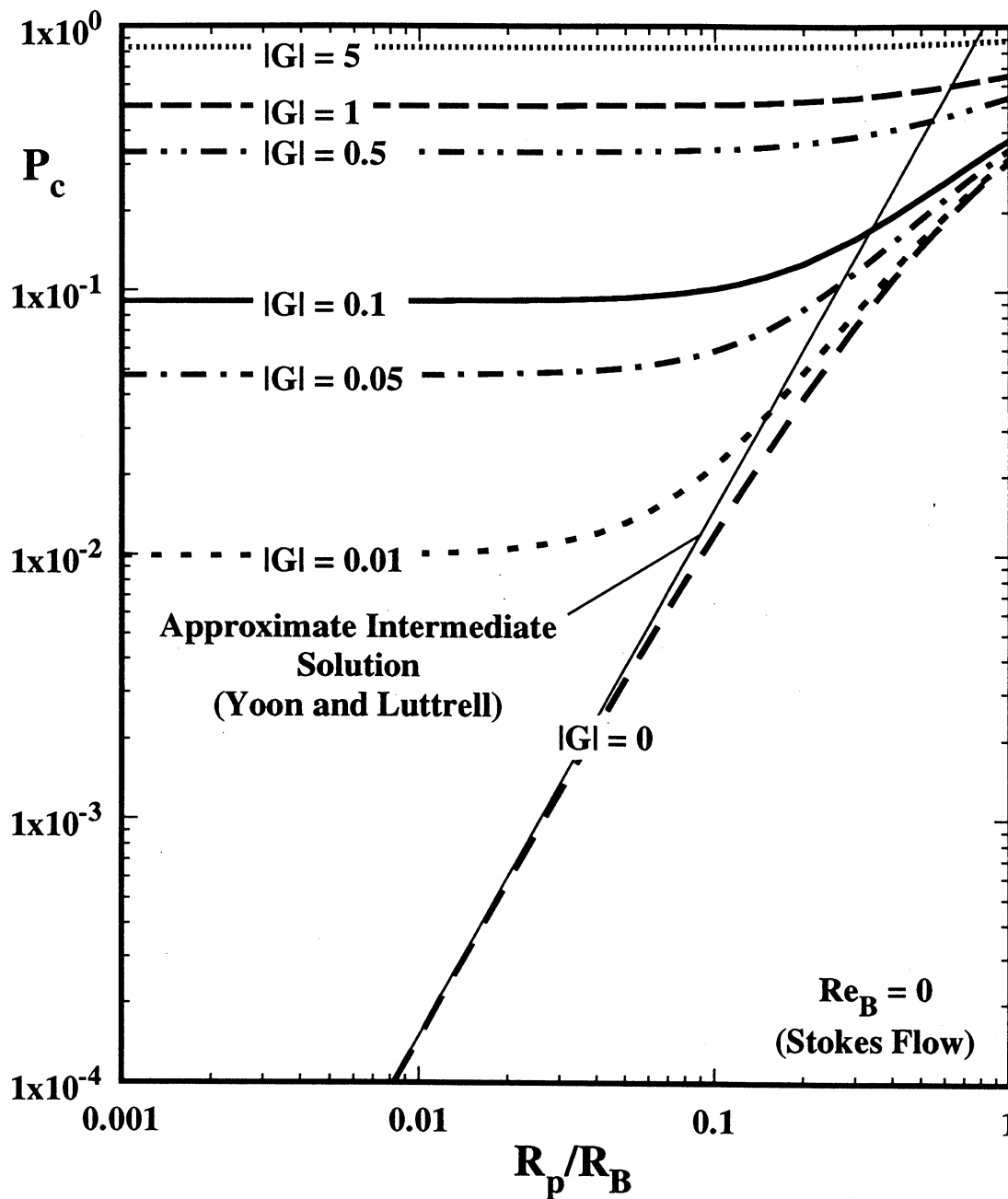


Figure 12: Exact  $P_c$  predictions for intermediate flow with  $0 \leq |G| \leq 5$  and  $Re_B = 0$ .

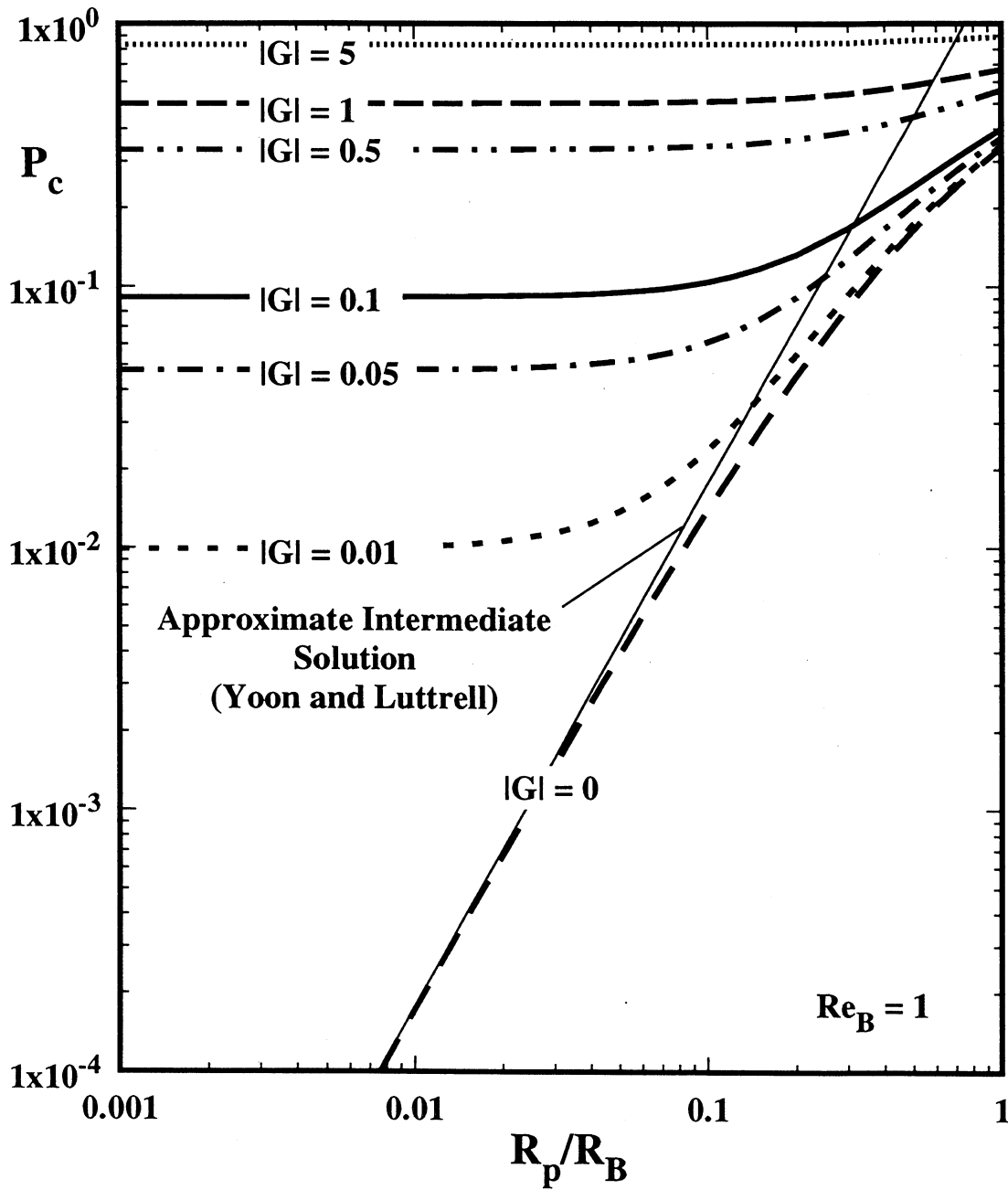


Figure 13: Exact  $P_c$  predictions for intermediate flow with  $0 \leq |G| \leq 5$  and  $Re_B = 1$ .

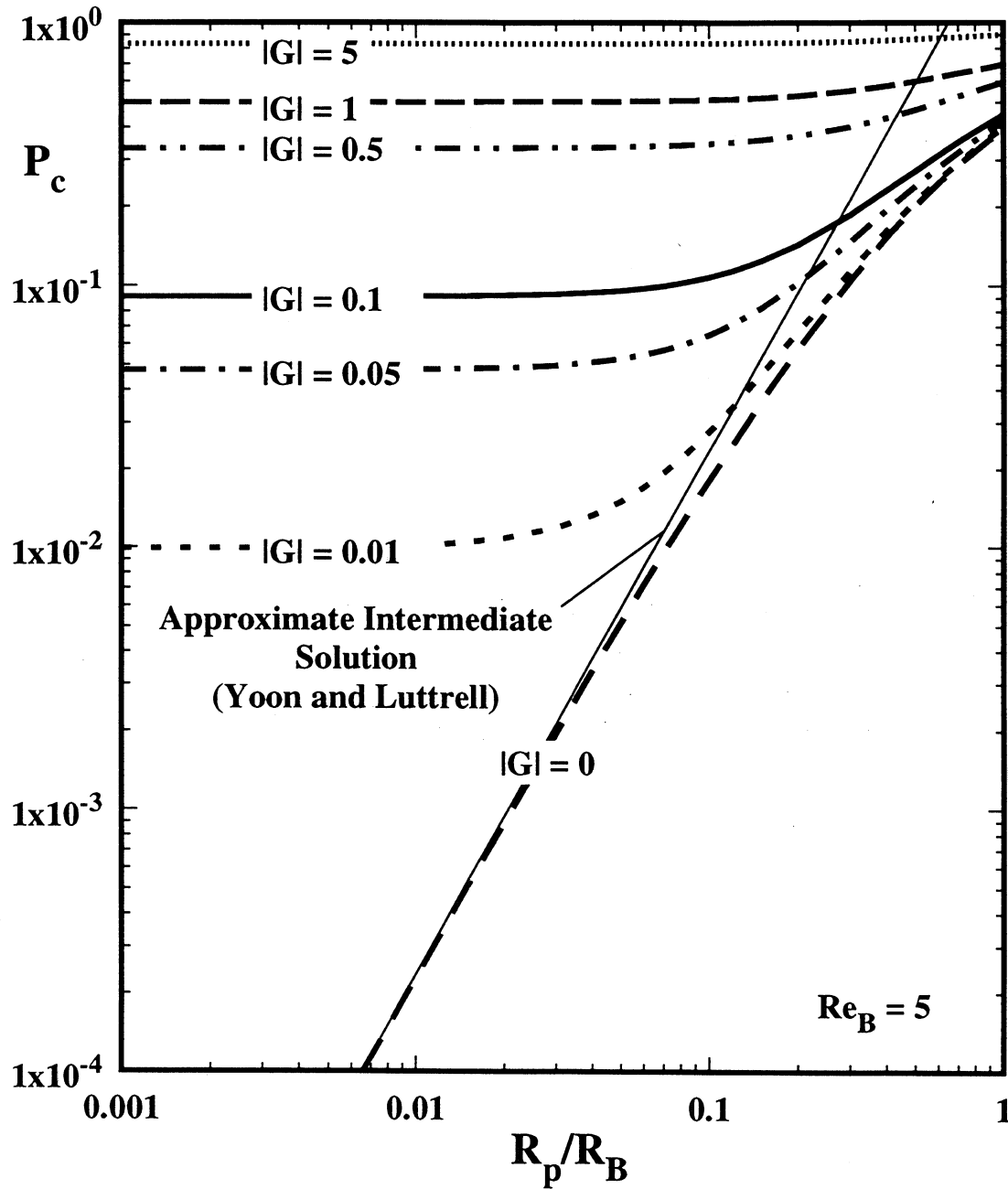


Figure 14: Exact  $P_c$  predictions for intermediate flow with  $0 \leq |G| \leq 5$  and  $Re_B = 5$ .

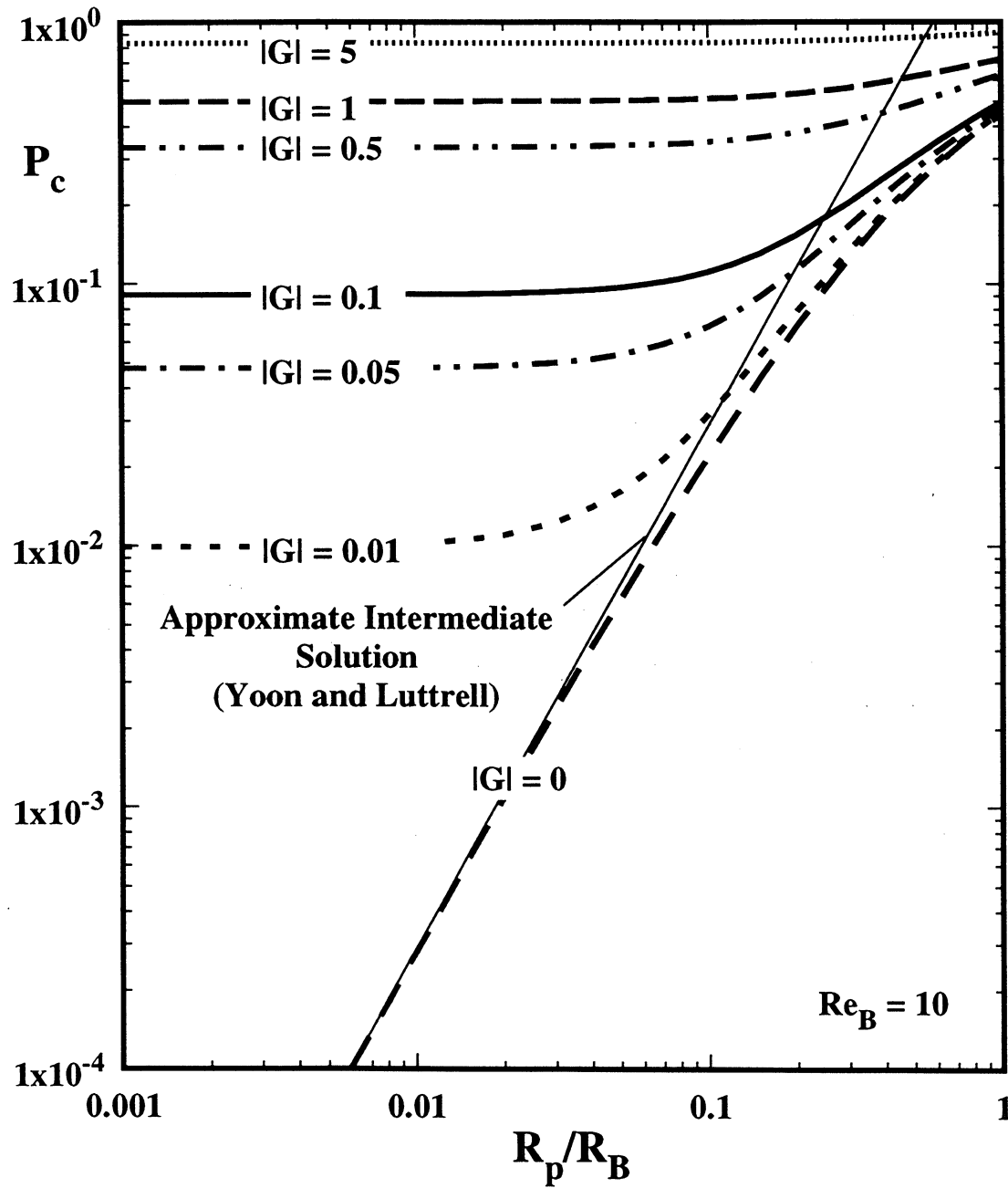


Figure 15: Exact  $P_c$  predictions for intermediate flow with  $0 \leq |G| \leq 5$  and  $Re_B = 10$ .

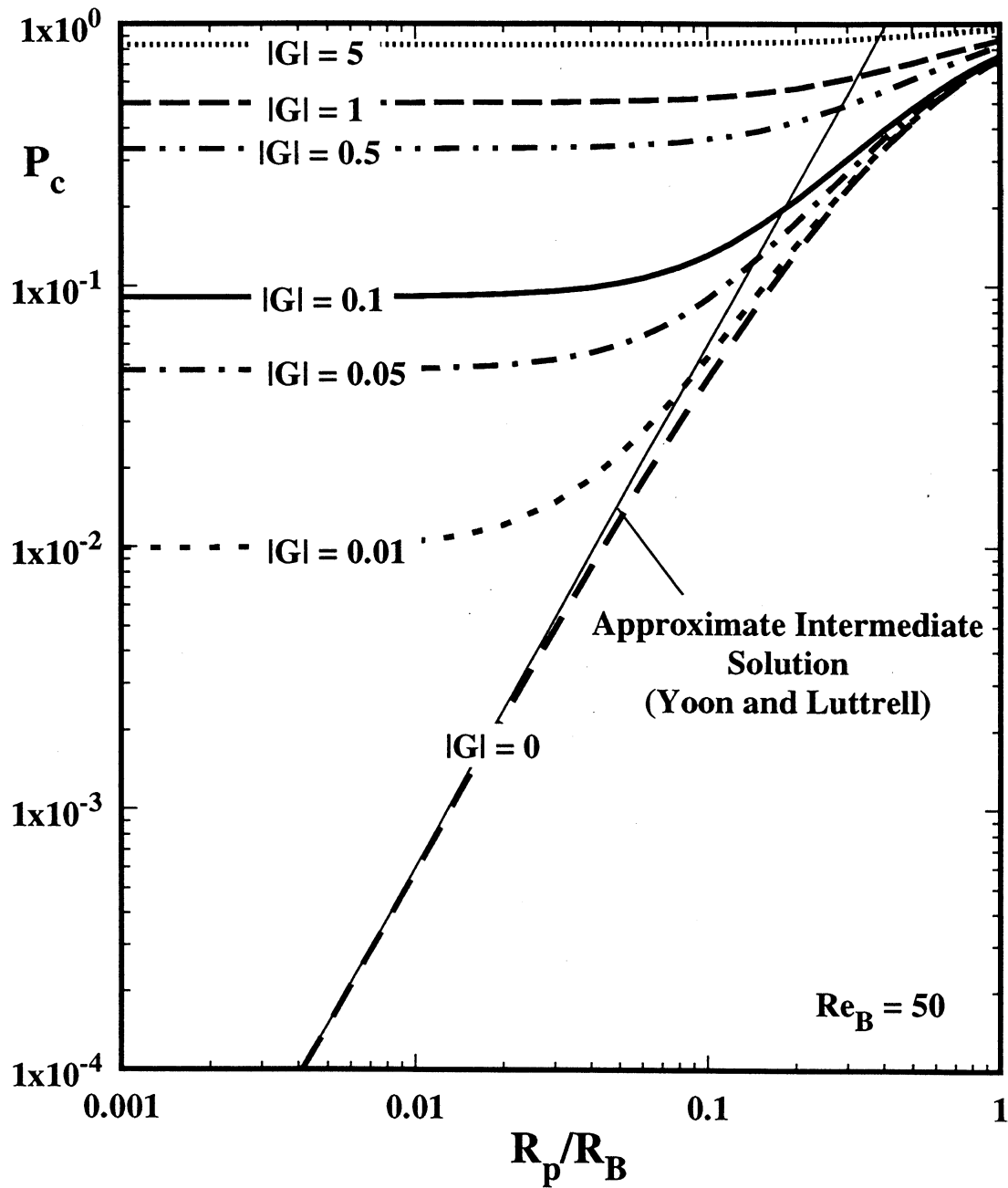


Figure 16: Exact  $P_c$  predictions for intermediate flow with  $0 \leq |G| \leq 5$  and  $Re_B = 50$ .

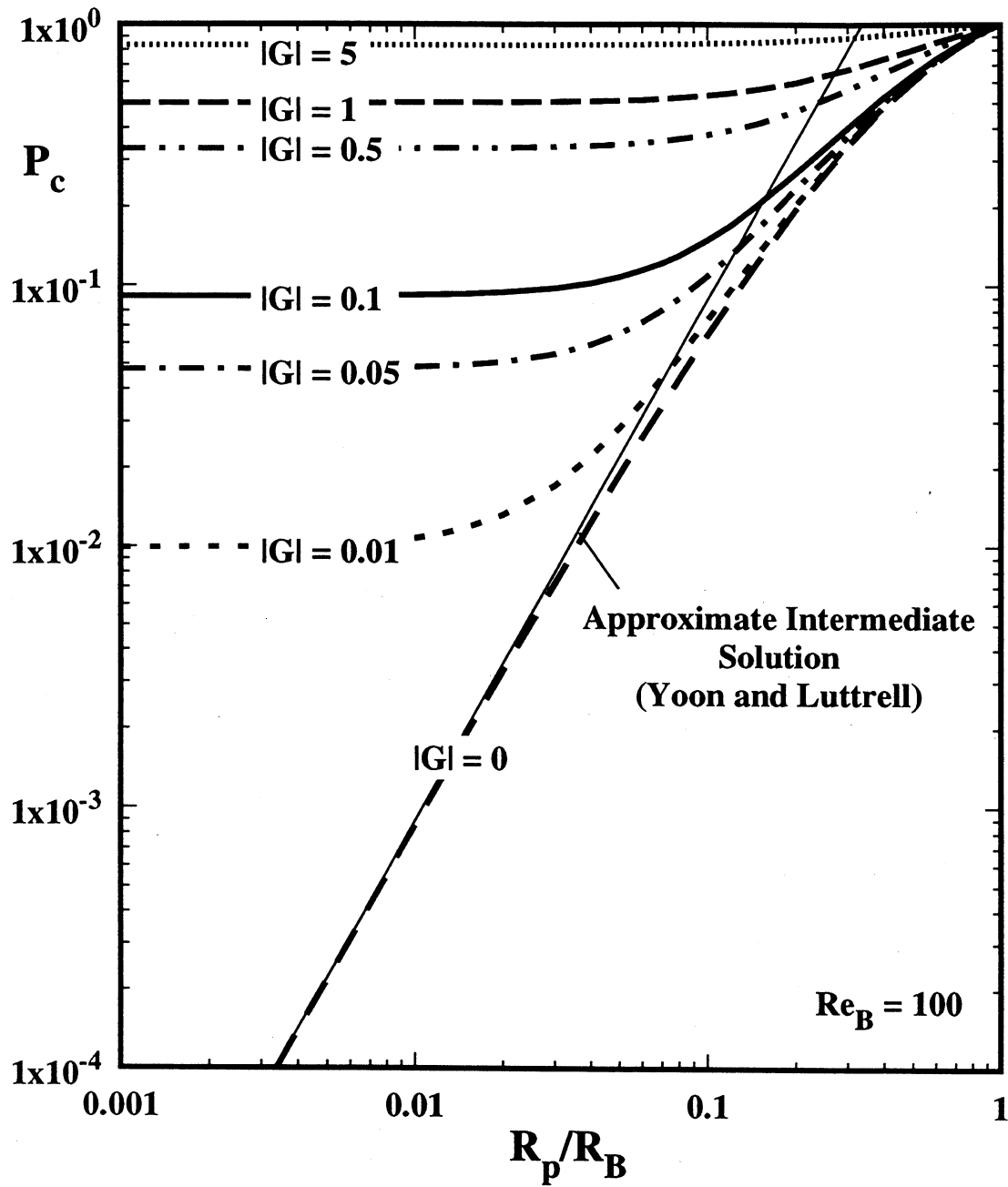


Figure 17: Exact  $P_c$  predictions for intermediate flow with  $0 \leq |G| \leq 5$  and  $Re_B = 100$ .

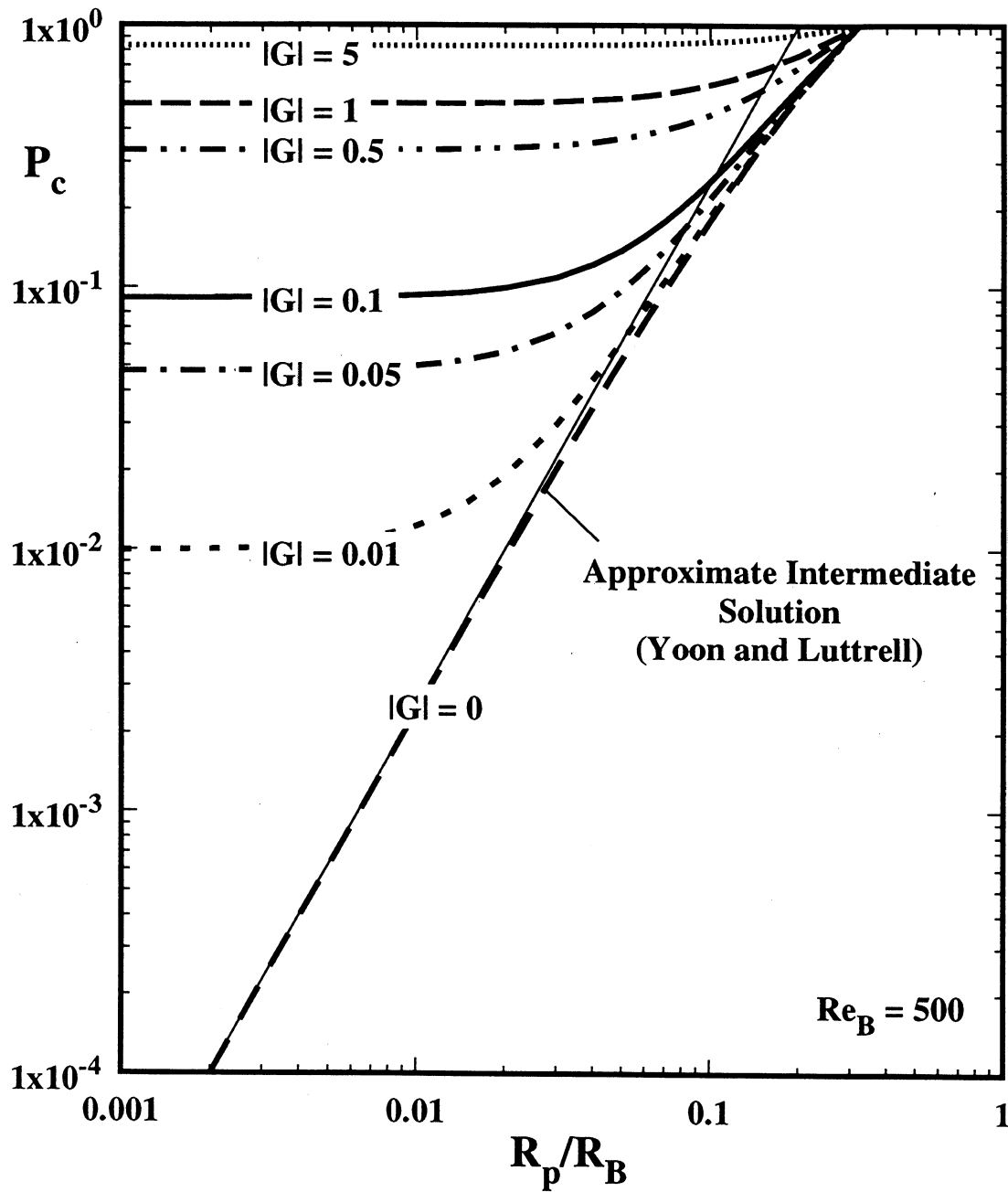


Figure 18: Exact  $P_c$  predictions for intermediate flow with  $0 \leq |G| \leq 5$  and  $Re_B = 500$ .

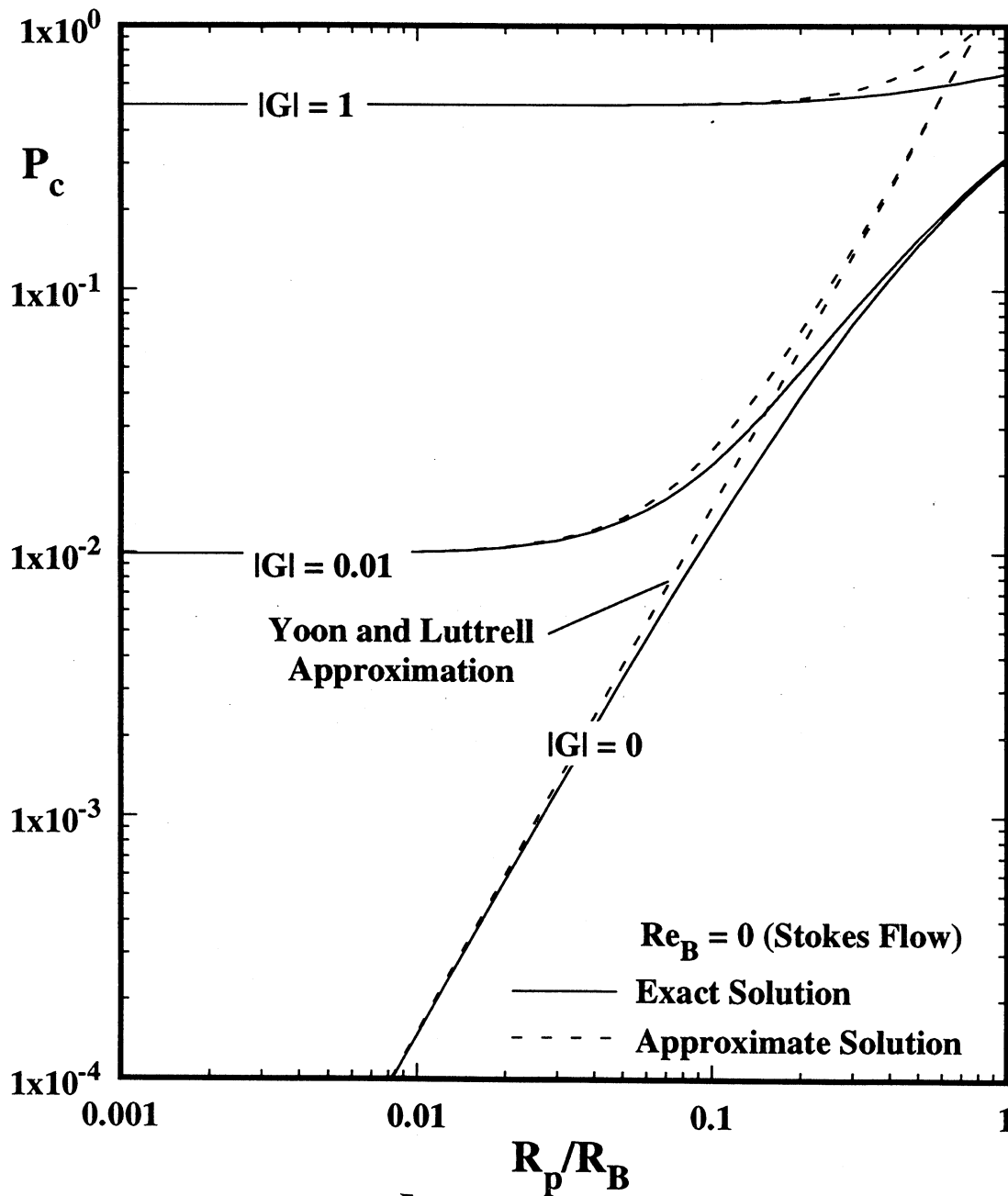


Figure 19: Exact and approximate  $P_c$  predictions for  $|G| = 0, 0.01, \text{ and } 1$  and  $Re_B = 0$ .

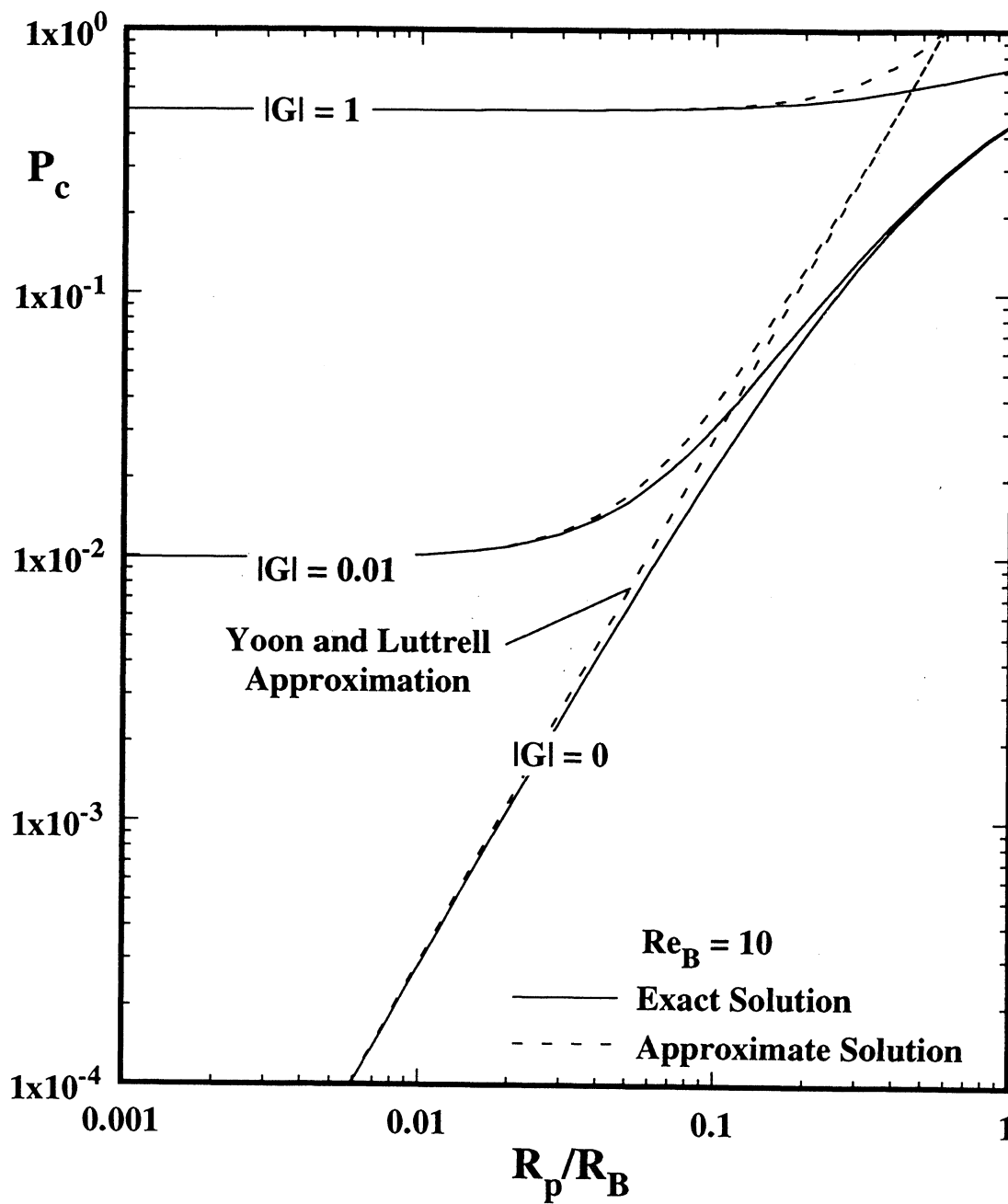


Figure 20: Exact and approximate  $P_c$  predictions for  $|G| = 0, 0.01, \text{ and } 1$  and  $Re_B = 10$ .

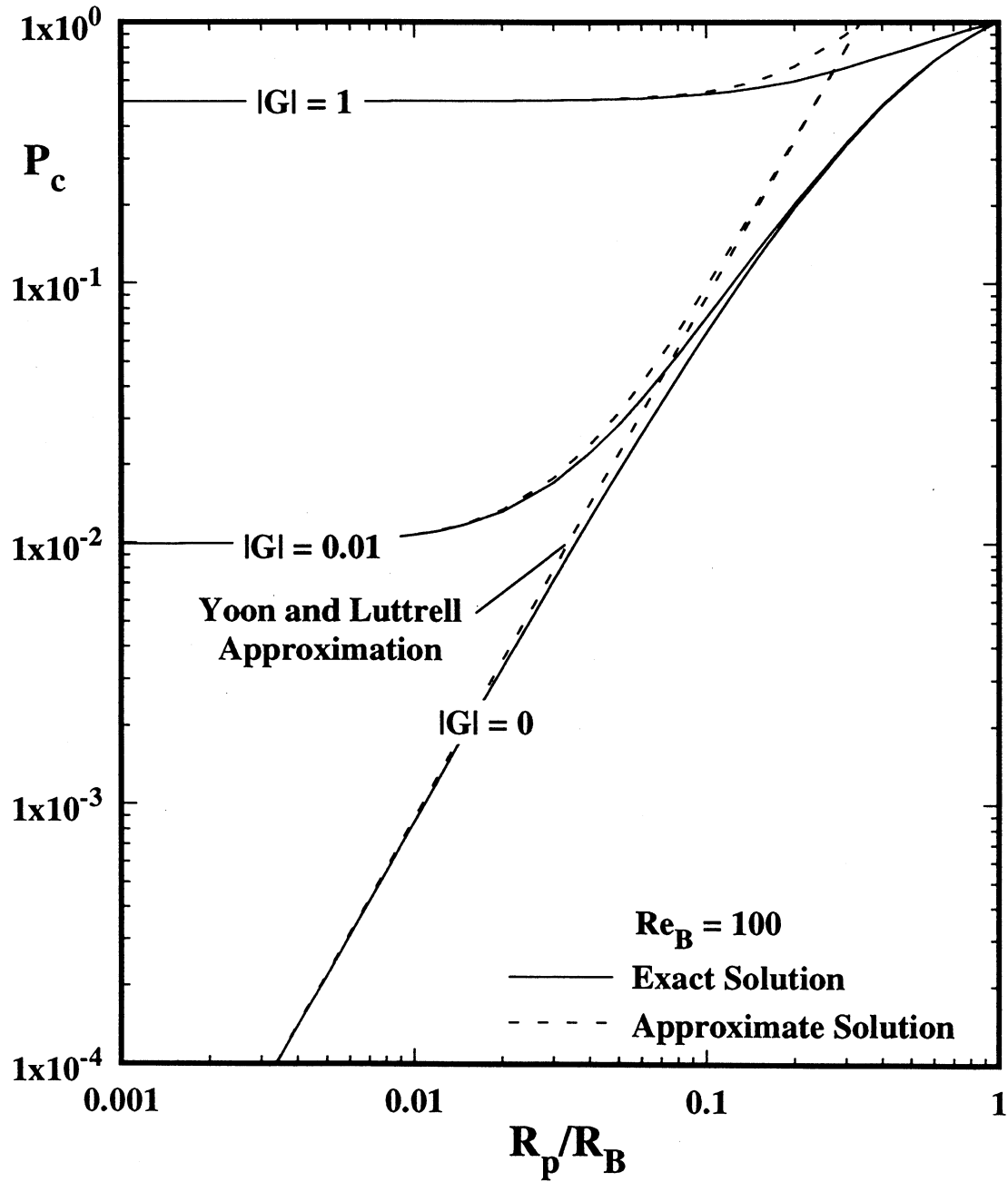


Figure 21: Exact and approximate  $P_c$  predictions for  $|G| = 0, 0.01, \text{ and } 1$  and  $Re_B = 100$ .

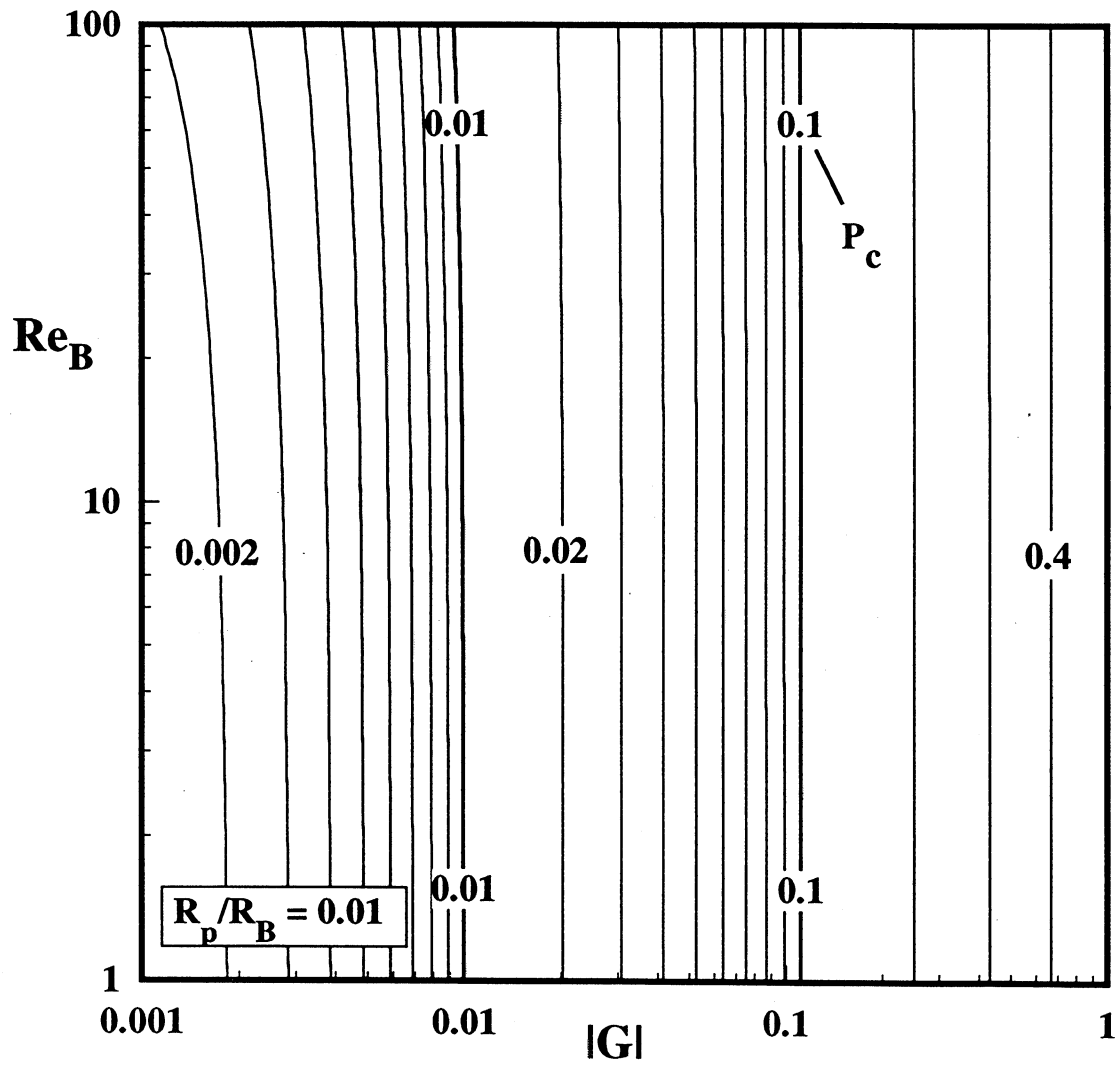


Figure 22: Contours of  $P_c$  when  $R_p/R_B = 0.01$ . Note that the  $P_c$  scale is logarithmic.

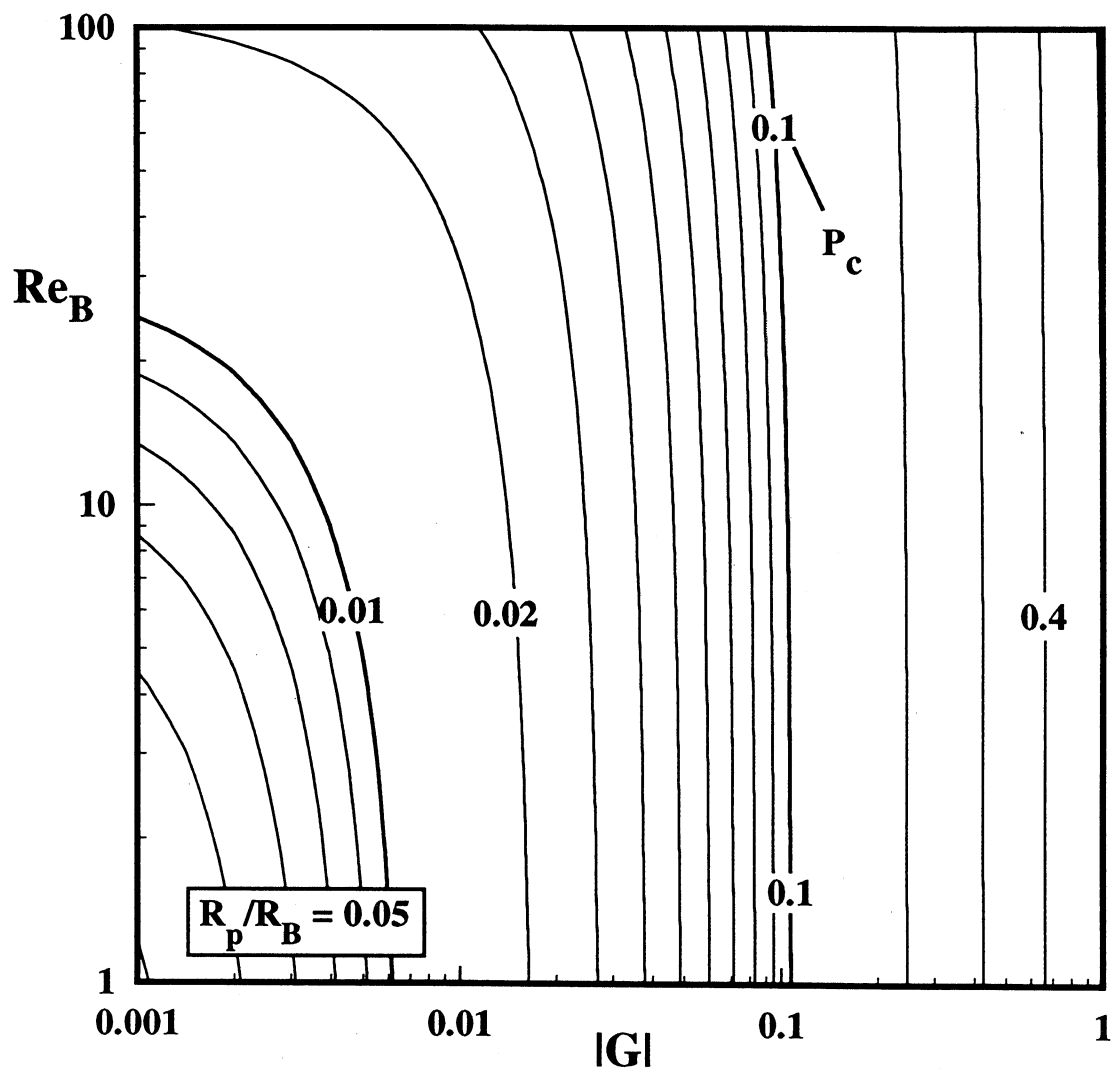


Figure 23: Contours of  $P_c$  when  $R_p/R_B = 0.05$ . Note that the  $P_c$  scale is logarithmic.

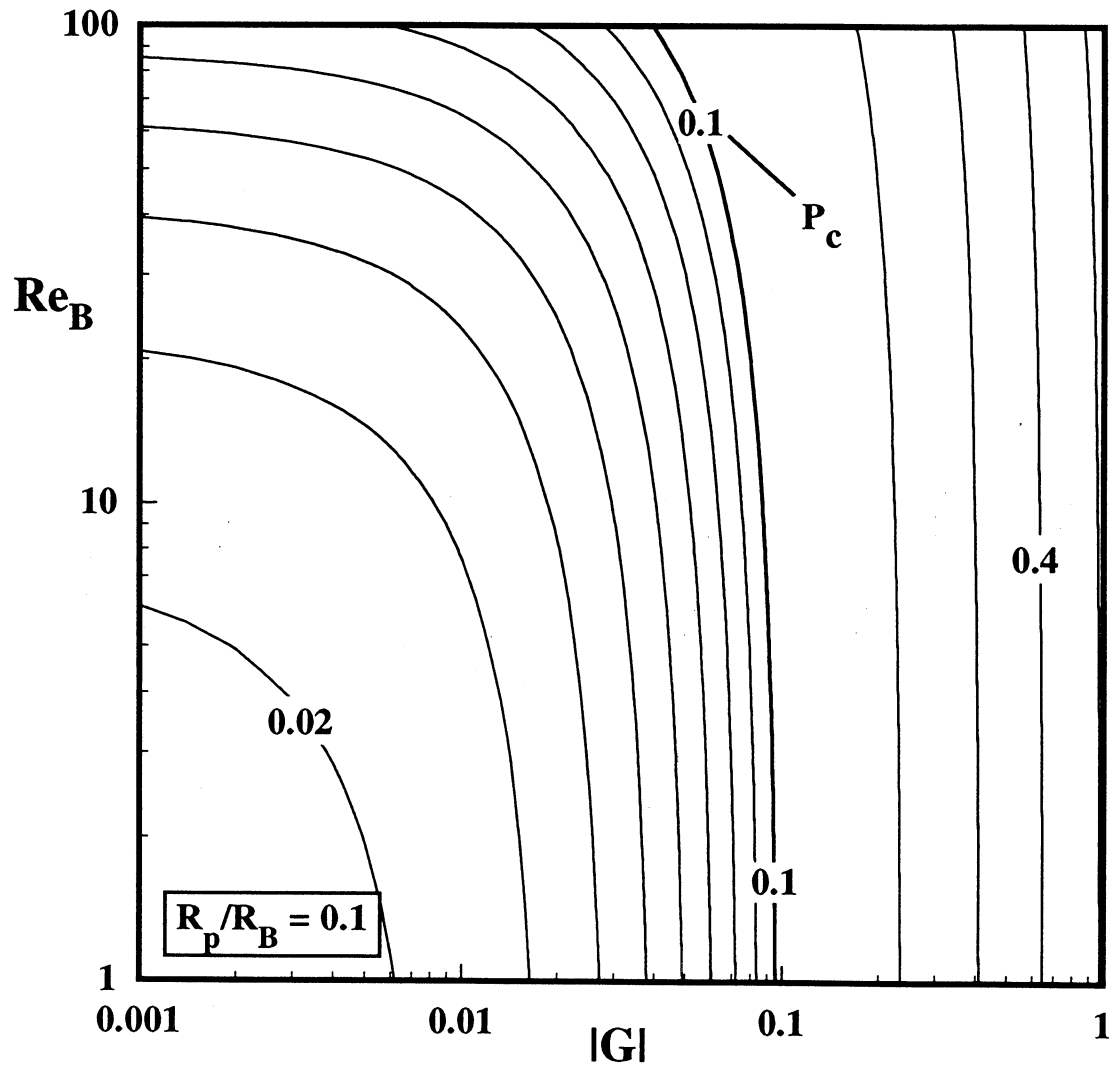


Figure 24: Contours of  $P_c$  when  $R_p/R_B = 0.1$ . Note that the  $P_c$  scale is logarithmic.

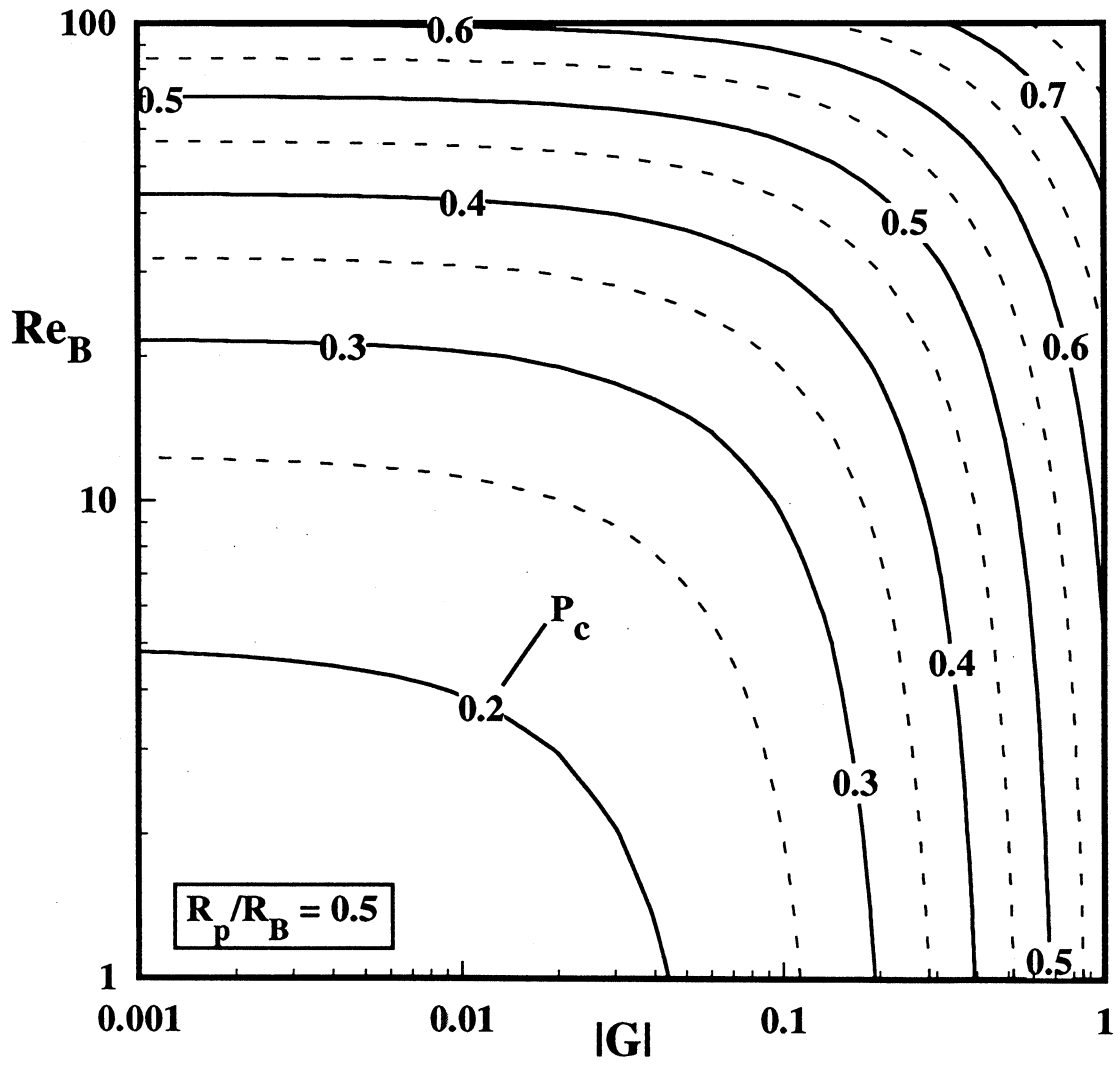


Figure 25: Contours of  $P_c$  when  $R_p/R_B = 0.5$ . Note that the  $P_c$  scale is linear.

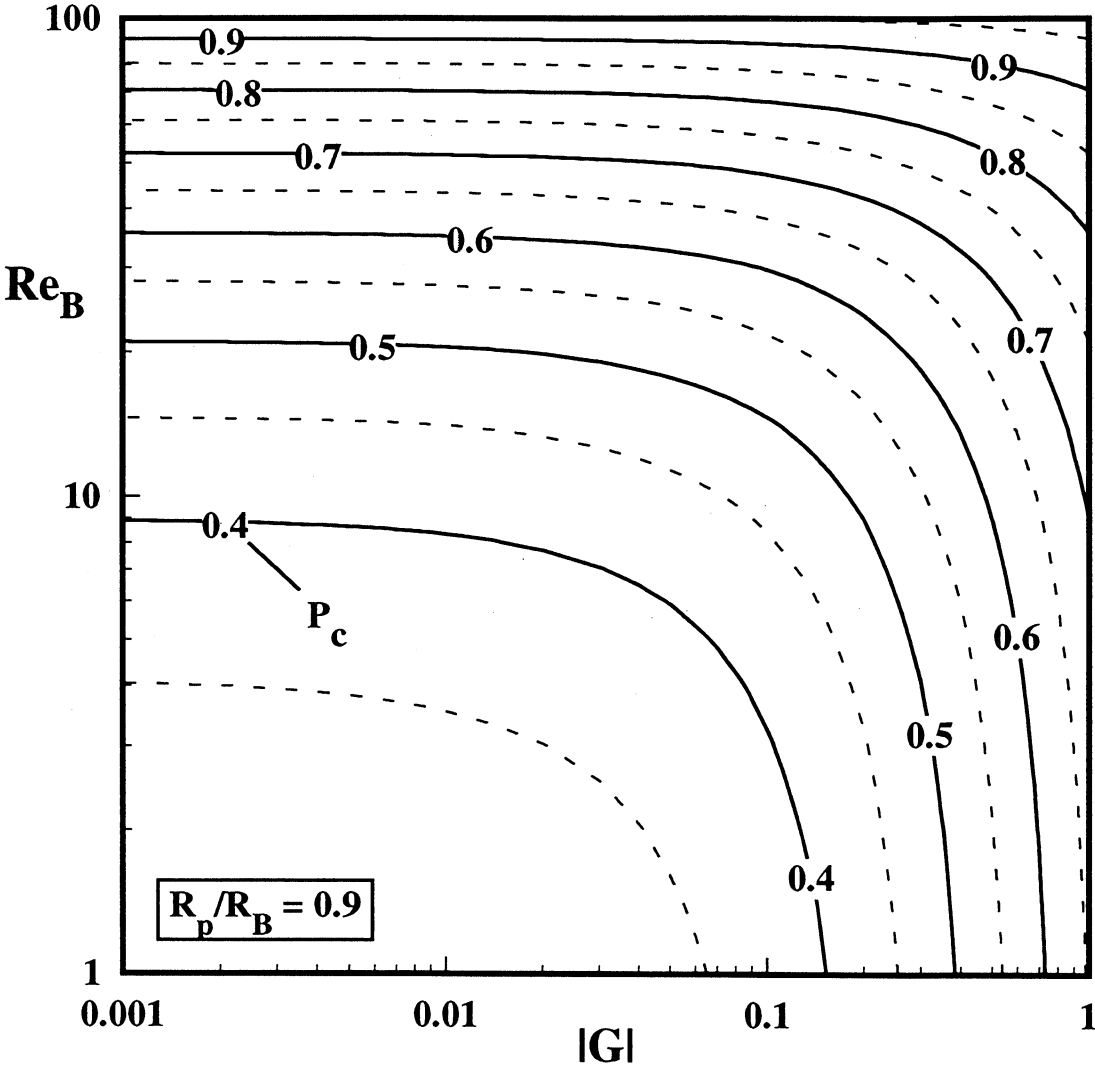


Figure 26: Contours of  $P_c$  when  $R_p/R_B = 0.9$ . Note that the  $P_c$  scale is linear.

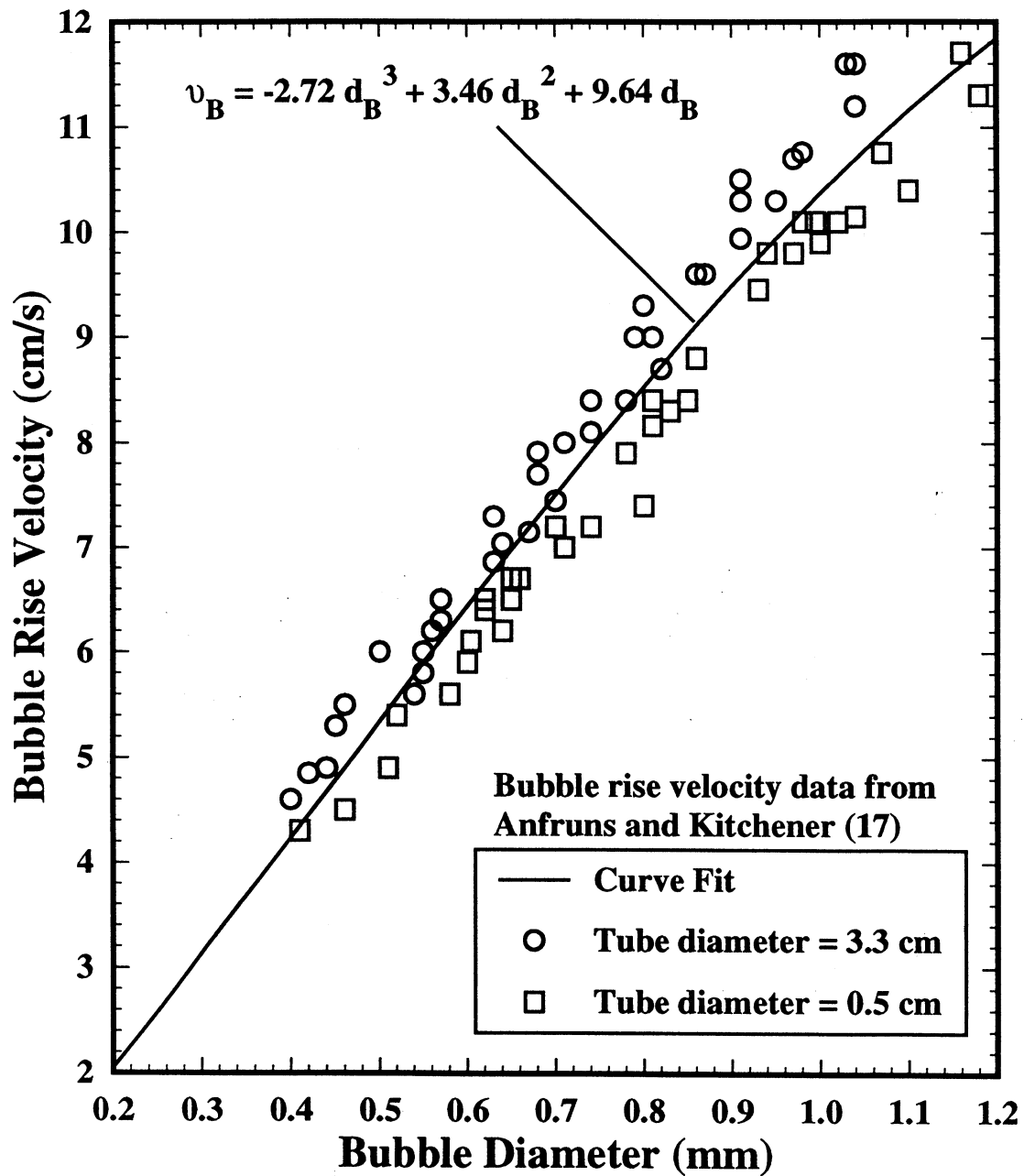


Figure 27: Bubble rise velocity data presented by Anfruns and Kitchener (17) and the associated correlation used in this report for the  $P_c$  predictions.

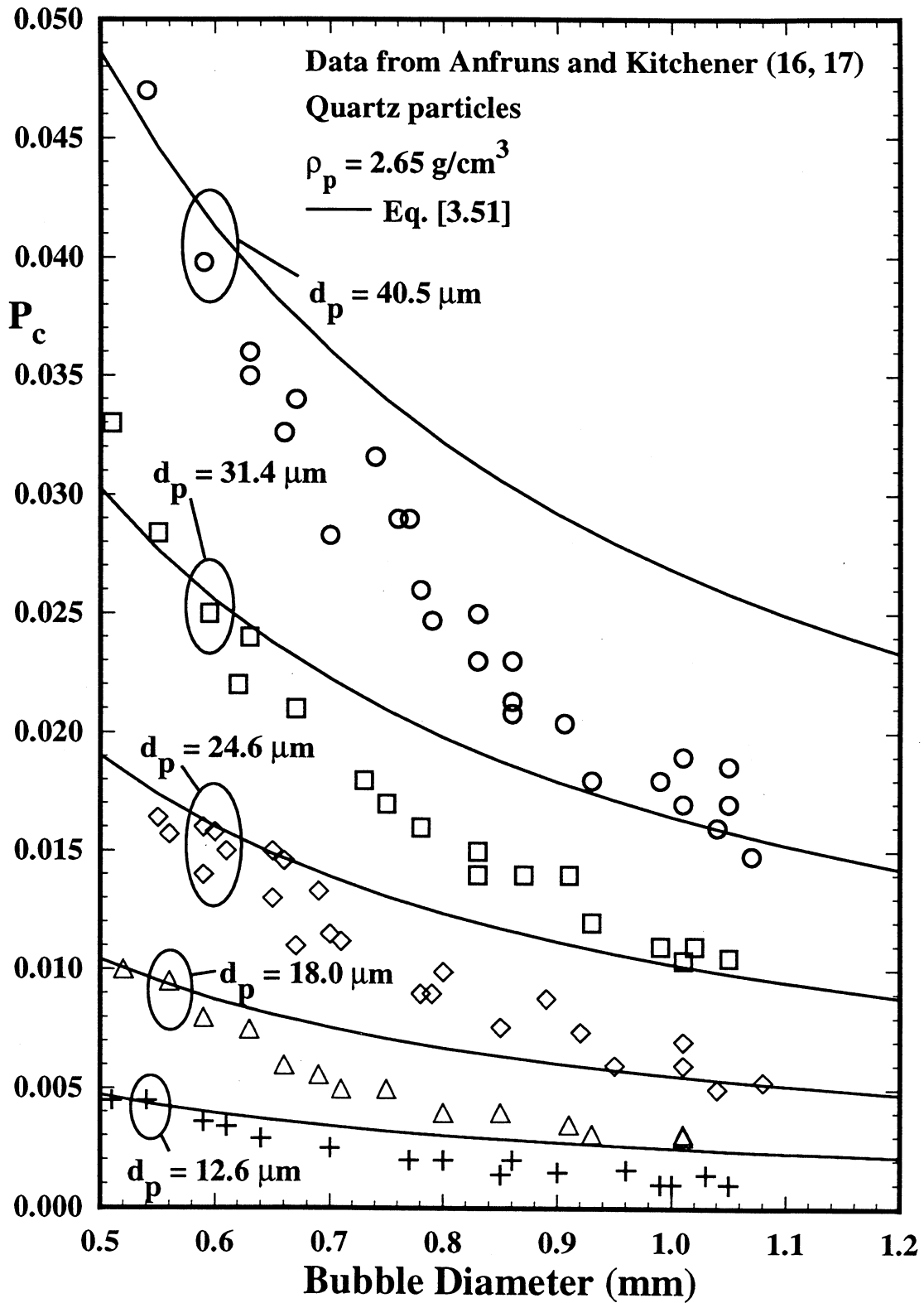


Figure 28: Experimental data for  $P_c$  obtained by Anfruns and Kitchener (16, 17) and the associated numerical predictions from the  $P_c$  model [3.51].

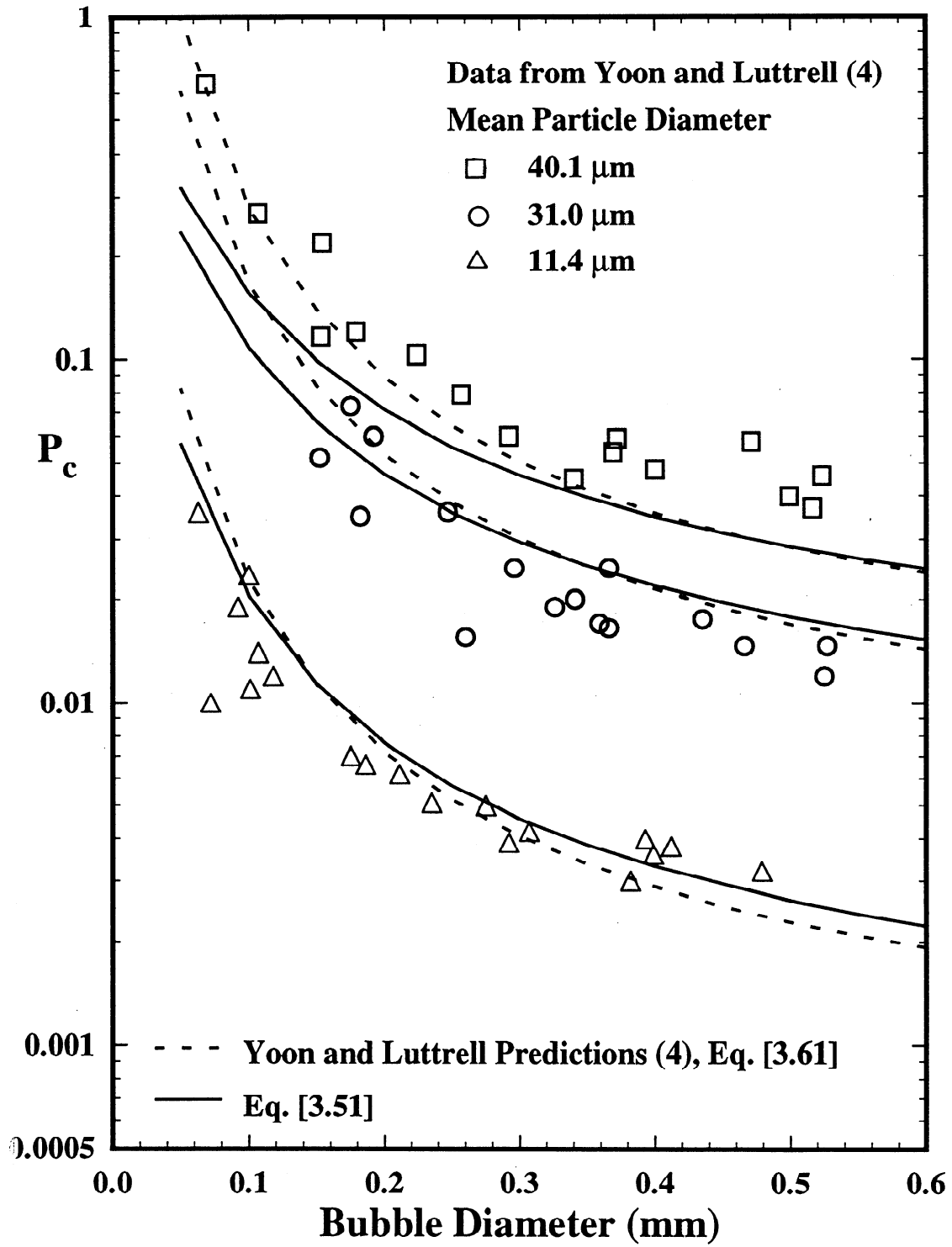


Figure 29: Comparisons between the experimental  $P_c$  data obtained from Yoon and Luttrell (4) and numerical predictions for  $P_c$ .

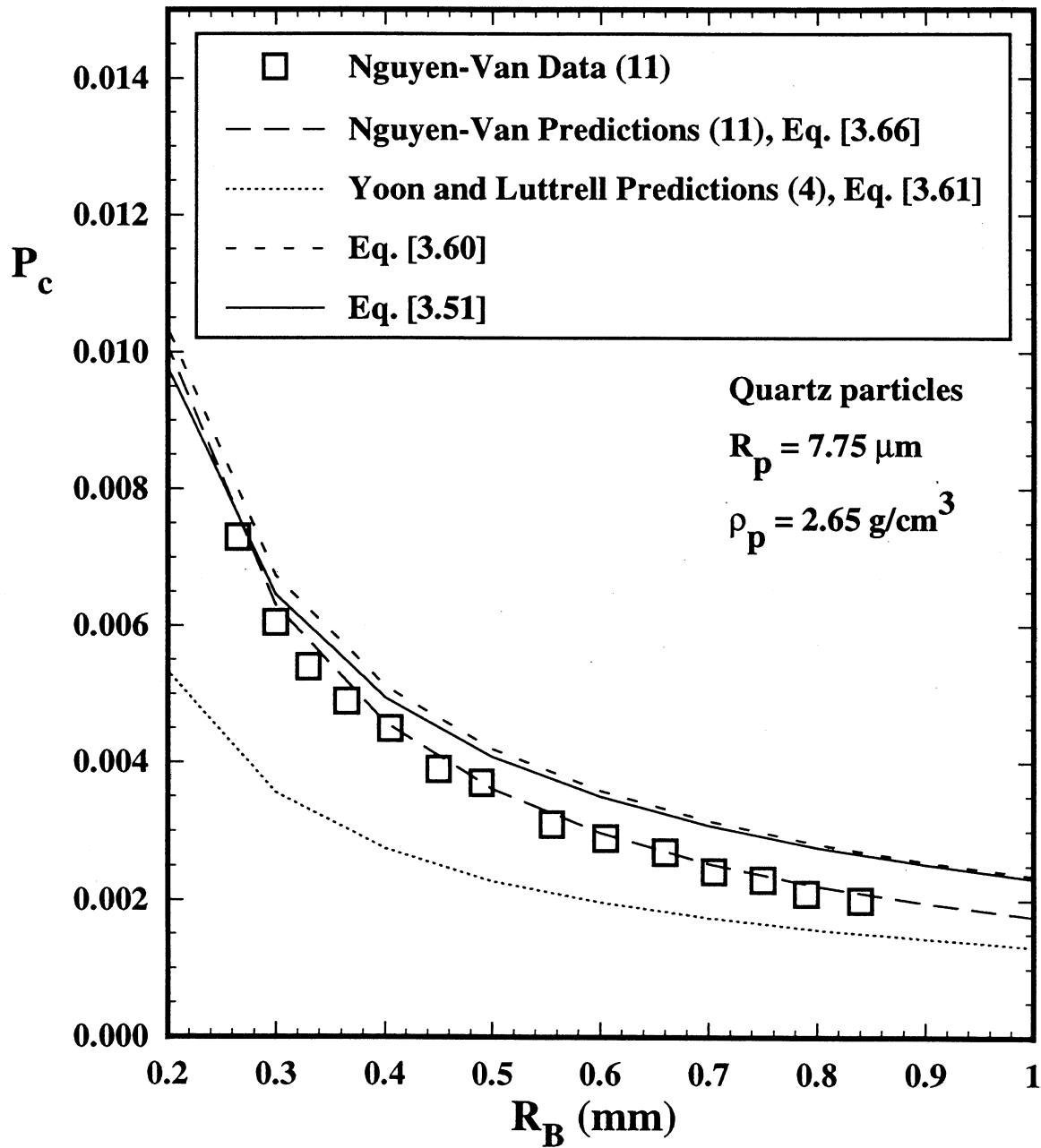


Figure 30: Comparisons between experimental and numerical values for  $P_c$  for quartz particles with  $R_p = 7.75 \mu\text{m}$ .

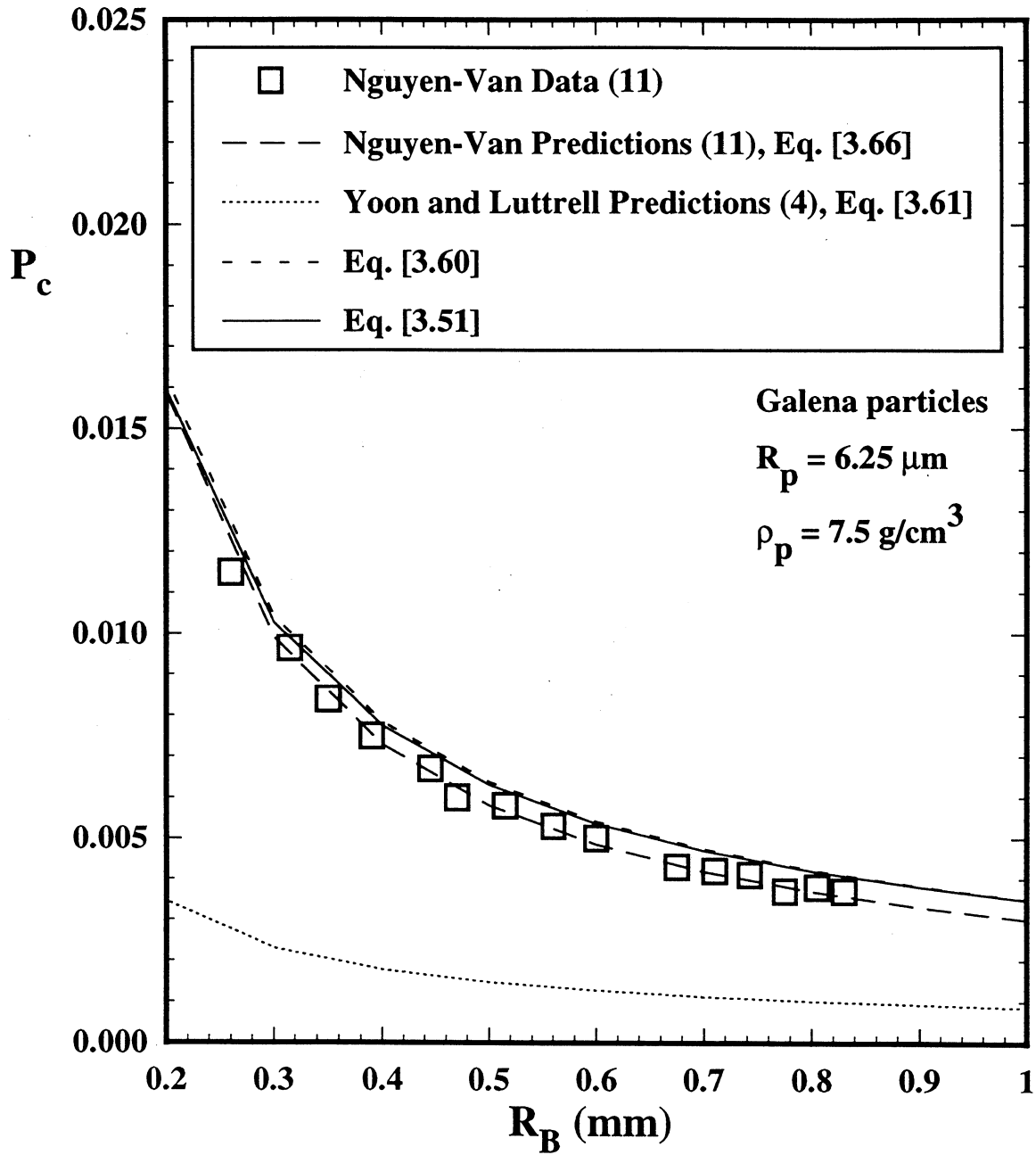


Figure 31: Comparisons between experimental and numerical values for  $P_c$  for galena particles with  $R_p = 6.25 \mu\text{m}$ .

